Maceral study to determine the desorbed gas content in the Upper Cretaceous coals of the Landázuri area, Middle Magdalena Valley Basin, Colombia

Clara Guatame (clara_guatame@hotmail.com)
Servicio Geológico Colombiano https://orcid.org/0000-0003-3101-6534
Marco Rincón
Servicio Geológico Colombiano
Mauricio Bermúdez
Universidad Pedagogica y Tecnologica de Colombia

Case study

Keywords: Middle Magdalena Valley, coal, petrology, maceral, gas, principal component analysis (PCA)

Posted Date: September 17th, 2021

DOI: https://doi.org/10.21203/rs.3.rs-885749/v1

Maceral study to determine the desorbed gas content in the Upper Cretaceous coals of the Landázuri area, Middle Magdalena Valley Basin, Colombia

Clara Guatame[a], Marco Rincón[b], Mauricio Bermúdez[c]

[a, b] *Servicio Geológico Colombiano, Bogotá, Colombia*

[c] *School of Geological Engineering, Universidad Pedagógica y Tecnológica de Colombia- UPTC*

[a] cguatame@sgc.gov.com, clara_guatame@hotmail.com

[b] mrincon@sgc.gov.co

[c] mauricio.bermudez@uptc.edu.co

ORCID 0000-0003-3101-6534; 0000-0002-4896-5384; 0000-0003-0584-4790

Abstract

For several decades, some coal petrographic properties have been proposed as important parameters in the methane gas sorption processes. In this contribution, the petrographic variables (Vitrinite Ratio, Inertinite Ratio, the petrographic indexes (Gelification Index, Groundwater Index, Tissue Preservation Index, Vegetation Index, Vitrinite/Inertinite ratio, and the Vitrinite Reflectance were evaluated according to the maceral preservation and were related with the desorbed gas content. Twenty-five coal seams obtained from the drill cores of two wells in the Landázuri Area-Valle Medio del Magdalena basin were analyzed. The coal samples were grouped according to gas content using principal component analysis (PCA). The petrographic results were analyzed by linear regression and multiple regression. The Medium Volatile Bituminous to Low Volatile Bituminous coals from Landázuri 1 are twice as high in gas content that the High Volatile Bituminous A to Medium Volatile Bituminous coals from Landázuri 2. The volume percentage and the preservation degree macerals are related closely to the gas content and the pore's size involved in the sorption process. The Inertinite is the maceral group related with the highest gas content groups in Landázuri (600 SCF-Standard Cubic Feet/ton, 300 SCF/ton), while the other groups show the correspondence with the vitrinite macerals. The syngenetic and diagenetic origin of the pyrite contributes microporosity to the desorption process, while the pyrite epigenetic by its size reduces it. The petrographic indexes reveal that the Upper Cretaceous coals were developed in swampy or lacustrine continental basins- limnic facies.

Keywords: Middle Magdalena Valley, coal, petrology, maceral, gas, principal component analysis (PCA)

Introduction

The Energy Resources group of the Servicio Geológico Colombiano has been conducting Coal Bed Methane (CBM) studies since 2011 in five Colombian coal areas. In 2016, total ash-free gas contents (37.54- 818.14 SCF/ton) were obtained from coal seams of the Umir Formation-Upper Cretaceous of the Landázuri area-Middle Magdalena Valley Basin. The resources potential was calculated as 360.47 BCF (Billion Cubic Feet) (Ortíz et al. 2016). Gas chromatography analysis indicated that the methane gas percentage is between 41.90% and 92.50% of the gas measured in the analyzed coal seams (Ortíz et al. 2016). The relationship between methane gas accumulation mechanisms and coal composition has led to the examination of certain measurements of interest in petrological analyses, which act during the process of hydrocarbon sorption.

The largest volume of CBM resources worldwide is found in the countries of Russia, China, United States, Canada, Australia, Indonesia, Poland, Germany, and France, corresponding to 4000-7011 trillion cubic feet, of which 1060-1500 trillion cubic feet are considered recoverable. The United States has been the leader in CBM production since the '90s with an upward trend, with 2008 being the only decrease year; while China and Australia substantially increased their own CBM production in 2010 and 2014, respectively, focusing on high-rank coals and with interest in natural gas liquids (NGL) production. Thus, it is expected that Australia will soon take the top spot on the global market, with India occupying 5th place (Mastalerz and Drobniak 2020).

In Colombia, coal is a primary source for electricity generation, being also the largest producer in South America, with 1.46 exajoules (EJ)- 50 million tonnes in 2020 (BP 2021). Coal reserves reported during 2020 equaled 4554 million tonnes of bituminous and anthracite coals (BP 2021). The Middle Magdalena Valley basin has been in the sights of explorers because of its high hydrocarbon potential. The first oil field discovered in the country is located. At the northeast of the basin is located the Opón River- Landázuri coal area. Its potential is 201,012,049 million tonnes (Mt) of thermal coal and 137,156,216 Mt of metallurgical coal from the Upper Cretaceous Umir Formation (Monroy and Sandoval 2014). In terms of CBM reserve estimation, the analysis of two boreholes (Landázuri 1 and Landázuri 2) allowed estimating a potential of 360.47 Billion Cubic Feet (BCF)

(Ortíz et al. 2016). The detailed petrological analyses are vital to know the coal composition and the geological mechanisms of accumulation of coal-associated gas in an area with high tectonic complexity.

Coal petrology studies began in Colombia from the year 2000 onwards in different areas of the country (Castaño and Gómez 2001; Guatame and Sarmiento 2004; Mejía et al. 2006; Blandón 2007; Gómez and López 2017; Guo et al. 2018; Akinyemi et al. 2020; Guatame and Rincón 2021, among others) mainly to contribute to the knowledge of the petrographic composition and the definition of the sedimentary environment.

Studies on CBM potential began in 1990 led by governmental entities and universities, including, Agencia Nacional de Hidrocarburos- ANH, Ecopetrol-Instituto Colombiano del Petróleo (ICP), Agencia Nacional de Minería (ANM), Servicio Geológico Colombiano (SGC), Ministerio de Minas y Energía (MME), Unidad de Planeación Minero Energética- UPME, Escuela de Administración, Finanzas e Instituto Tecnológico-EAFIT Universidad Industrial de Santander-UIS, Universidad Pedagógica y Tecnológica de Colombia- UPTC, and Universidad Nacional de Colombia sede Medellín, among others (Mariño et al. 2015). In addition, the Drummond company stands out for carrying out the first CBM exploitation project in the Cesar Ranchería basin. In the before-mentioned studies, no petrological analysis of coal was performed, and in many of them, an analysis of the influence of coal composition on methane gas content was not rigorously elaborated. However, Mariño and Mojica (2014) carried out a petrographic study in the Amagá basin on low-rank coals and concluded that the vitrinite maceral group is the most influential component for gas adsorption and that the mineral matter content evidences an inverse relationship concerning gas content since it acts as a diluent.

Furthermore, under a significant number of studies from the sedimentary basins of China, Australia, Canada, and the United States, crucial variables that influence the sorption capacity of methane gas in coal seams to have been defined: the range and burial depth (e.g., Laxminarayana and Crosdale 1999; Wang et al. 2011; Bustin and Bustin 2016; Busch et al. 2019), the maceral composition (e.g. Yao et

al. 2009, Jian et al. 2015; Li et al. 2016; Hou et al. 2017), the pore size distribution (micro, macro, mesoporous), and the specific surface area (e.g., Crosdale et al. 1998; Laxminarayana and Crosdale 1999; Chalmers and Bustin 2007; Busch and Gensterblum 2011; Li et al. 2014; Jian et al. 2015). According to the notion that the most frequent maceral groups are Vitrinite and Inertinite, some authors claim that macerals of the Vitrinite group present higher adsorption capacity and higher desorption rate (e.g., Crosdale et al. 1998; Laxminarayana and Crosdale 1999, among others). Others (Wang et al. 2011; Jian et al. 2015; Wang et al. 2018; among others) express that it is the inertinitic macerals that have this capacity. Regarding the mineral matter content resulting from the coal formation processes, some authors indicate its relationship with the gas adsorption capacity (e.g., Laxminarayana 1999; Moore 2012; Raharjo et al. 2018), with the desorption rate (e.g., Crosdale et al. 1998; Li et al. 2017) and with the porosity contribution in the sorption process (e.g., Bertrand 1989).

Colombian research on CBM potential has targeted different coal areas and has yet to properly analyze the close relationship between the gas contents obtained and the origin of the coal (Mariño and Mojica 2014). The research challenge is to define which are the inherent physical properties of coals (rank, maceral composition, mineral composition, facies, pore structure) involved in the higher or lower gas content, which is necessary for the exploration of new economic alternatives for coal deposits.

The main purpose of this study is to establish the relationship between the measured gas content (SCF/ton) in the coal seams of the Landázuri 1 and Landázuri 2 wells, and the maturity degree of the petrographic composition, and in particular, the coal constituents that by their nature, preservation and the occurrence mode, contribute to gas sorption. This research also aims to define a methodology in exploratory studies of methane gas. Coal petrology is implemented as a prognostic discipline that provides the necessary elements in the CBM potential promising areas for the identification and prevention of gas-related accidents in mining operations. Petrophysical studies of porosity and permeability are not in the scope of this study.

Geological setting

The Landázuri 1 and 2 wells are located in the Armas syncline of the Río Opón-Landázuri coal-bearing area (Landázuri- Vélez area) along the eastern margin of the Middle Magdalena Valley basin (Fig.1). The area is affected by two regional thrust fault systems resulting from the Mesozoic rifting of northern Colombia and its subsequent reactivation during the Cenozoic for the time of the Andean orogeny (e.g., Colleta et al. 1990; Dengo and Covey 1993; Cooper et al. 1995, for more references see Sarmiento et al. 2015). The oblique compressional stress generated structures and reactivated transpressive faults generating second-order folds oblique to these main faults (Gómez et al. 2008 in Ortíz et al. 2016).

In the research area, the La Salina fault system corresponds to a reverse system with westward vergence spans from south to north in the western flank of the De Armas syncline putting in contact Maastrichtian rocks with those dated Lower to Middle Oligocene (Sarmiento et al. 2015; Ortíz et al. 2016). The Landázuri Fault system with westward vergence corresponds to a thrust scale of the La Salina Fault, located on the eastern flank of the syncline where Turonian rocks overlying Maastrichtian rocks. (Ortíz et al. 2016). The Armas syncline corresponds to a broad and asymmetric fold with southeast-northwest direction and widening on the eastern flank (Ortíz et al. 2016).

In the Upper Cretaceous rocks, the roughly 1400 meters thick Umir formation (Gómez et al. 2008 in Ortíz et al. 2016; Sarmiento et al. 2015) was deposited in a restricted marine environment with the development of marshy areas that accumulate organic matter for the subsequent production of economically exploitable coal seams (Sarmiento et al. 2015). The unit consists of three levels. In the Landázuri area the thickness is tectonically affected and the lower level of the Umir Formation or La Renta Formation- (Terraza 2020) is not evident. The middle level is 400 meters thick composed of a gray claystone succession with gray to light brown silty claystone intercalations and sporadic levels of very fine to fine-grained arenite. The segment has coal seams with variable thicknesses ranging from a few centimeters to 3 meters. The upper level is 400 meters thick and consists of a succession of light brown, intercalated with gray clayey siltstones and coal seams of fine-grained arenite (Ortíz et al. 2016).

The Landázuri 1 well is located on the eastern flank of the De Armas syncline in the southern sector, crossing the upper and middle levels of the Umir Formation. Fourteen coal seams numbered from base to top (M3- M23) were analyzed according to the stratigraphic position with variable thicknesses ranging from 0.40 m to 2.63m (Ortíz et al. 2016). The Landázuri 2 well is located northwest on the western flank of the syncline. On the middle level, eleven coal seams were identified (M2- M18) with thicknesses varying from 0.55 m to 2.38 (Ortíz et al. 2016) (Fig. 1 and 2).

Experimental methods

Gas measurement method

The gas desorption measurement of the cores was performed through the direct canister method, as desorbed and residual gas as a function of time and under pressure and temperature conditions that simulate the reservoir characteristics in a laboratory environment (Ortíz et al. 2016).

The coal degassing (lost gas) on the drilling cores consisted of the water displacement measurement in a volumetric column. After 24 hours, the measurement of desorbed gas was started in hermetically sealed canisters with in situ pressure and temperature control or calculated with the geothermal gradient. The absorbed gas by the coal matrix was calculated from the residual gas in pulverized samples (60 mesh) in a container for gas mixture or in a hermetically sealed ball mill connected to a manometer. The measurements obtained were processed using the TerraGas software (https://terrasolid.com/product/tgas/), which performs pressure, temperature, and gas volume corrections, measured from the sample weight, canister volume, volume of inert material introduced, and density (ISO Standard 17892-2:2014). The cumulative gas desorption curve points out the intervals of lost, measured and residual gas by plotting the cumulative gas content vs time (ft/ton Vs √hours) (Fig. 3). The ash correction was performed finally obtaining the ash-free total gas content. (Ortíz et al. 2016). Gas chromatography was used to determine the percentage of gas mixture and methane gas in the measured contents of each sample (Ortíz et al. 2016).

Petrographic methods

The reflectance values (Ro) were obtained by professionals from the Servicio Geológico Colombiano's Laboratory of Characterization, Processing and Research of Coal and Energetic Materials, according to the ASTM D2798-05 standard. The identification and classification of the macerals was carried out according to Standard D2799-05 with the reading of 500 points in each specimen and its corresponding repeatability. A Leitz Ortholux II POLMK microscope was used with a magnification of 400x, a dot counter, and a mechanical stage that advances with fixed increments. The macerals classification used the nomenclature compiled by ICCP (1998, 2001) and the Pickel et al. (2017) nomenclature for the Liptinite group. The macerals of the Vitrinite and Inertinite groups were differentiated according to their degree of preservation (Lamberson and Bustin 1993). Structured Vitrinite is composed of the Telovitrinite and Gelovitrinite subgroup and the degraded Vitrinite is constituted of macerals of the Detrovitrinite subgroup. Preserved Fusinite and Semifusinite were counted as preserved inert, and the other macerals group make up the degraded inerts subgroup. The mineral matter was quantified as clay, pyrite, and others. The Pyrite classification was according to its formation process in coal as syngeneic, diagenetic and epigenetic. The coal facies were obtained from the application of petrographic indices proposed by Diessel (1986) and Calder et al. (1991).

Statistical methods

To avoid the analyst's subjectivity when classifying coal seams groups, cluster analysis was used, based on K-Means Clustering (Hartigan and Wong 1979). This procedure attempts to discriminate groups of relatively homogeneous cases, based on certain selected properties. In our particular case, the following variables were used: RV, RI, GI, GWI, TPI, VI, V/I. Pseudocode written in R was used, which allows a large number of cases to be considered. However, it is often the case that the algorithm requires the user to specify the number of clusters. For this, the initial number of the clusters was obtained from the Elbow Method (Lloyd 1982). In the algorithm, the initial centroids of the clusters can be specified, and the

cluster centroids are updated iteratively. The algorithm used also allows automatic selection of the number of clusters based on Bayesian information criteria (Schwartz 1978). It can also store cluster labels for each measurement, distance information, and the centers of the final clusters. The relative size of the statistics provides information about the contribution of each variable to the separation of the clusters. Once the classification is performed; the results are presented in the form of dendograms. The R correlation factor is analyzed as a linear regression product from the petrographic variables concerning the gas content in the defined groups. Then, for each group, a Pearson correlation coefficient analysis was carried out (Kendall and Stuart 1973), which allowed us to determine different relationships between variables pairs. The most significant variables from this independent study were compared statistically with each petrographic variable. Finally, the stepwise multiple regression method was applied, in which the contribution of each predictor variable to the response variable was analyzed. The algorithm determines which are the most important predictor variables for each one of the analyzed wells.

Results and discussion

Gas content

The ash-free gas total content results (Ortíz et al. 2016) in the twenty-five coal seams analyzed ranges between 37.54- 818.14 SCF /ton. The lowest value corresponds to M-15 from the Landázuri 2 well and the highest value measured at M-3 from the Landázuri 1 well.

Petrographic analysis

To the southeast of the De Armas syncline (see Fig. 1), the average reflectance of the Vitrinite ranges between 1.22- 1.86% MVB-LVB for Landázuri 1. The measured gas content fluctuates between 80.66 -818.14 SCF/ton, where 78.90-91% of the values obtained correspond to methane gas. To the northwest of the structure, coals are classified as HVBA- MVB for Landázuri 2 with values between 0.9 and 1.26% reflectance. The measured gas content is in the range

37.54 -484.88 SCF/ton, where 41.90- 92.50% of the obtained values correspond to methane gas (Ortiz et al. 2016; see Tables 1 and 2).

After having undergone the desorption process, the macerals showed numerous empty spaces of irregular size and shape. As shown in Tables 1 and 2, the Vitrinite content ranges between 65.71% and 94.03% in the analyzed samples. Likewise, the highest values correspond to the subgroup Detrovitrinite (Colodetrinite, Vitrodetrinite) and Gelovitrinite (Gelinite Colodetrinite involves different macerals such as Inertodetrinite and is observed partially fusinitized and devolatized (Fig. 5c, 5f, 5k, 5l, 5n, 6c, 6f, 6h). Gelinite is of a homogeneous aspect and is occasionally fractured (Fig. 5e, 6d), Vitrodetrinite is observed as angular fragments and is concentrated in the edges of the Vitrinite macerals (Fig. 5j, 6e).

The macerals content of the Inertinite group varies between 5.97-34.07% in the analyzed coal seams. Inertodetrinite is the most abundant maceral and is observed contained in Colodetrinite mainly (Fig. 5f, 5m, 6f, 6i). Fusinite and Semifusinite were quantified as preserved macerals-preserved cell structure and degraded-no cell structure (Fig. 5e, 5m, 54n, 5o, 6h, 6k). The macerals empty spaces may be empty or with mineral matter filling (Fig. 5e, 5g, 5i, 5b, 6g, 6h, 6j, 6k). The Liptinite content is very low or zero, and therefore, the maceral group was not analyzed.

The mineral matter comprises clay filling, replacing macerals (Fig. 5a, 5d, 6a, 6c) and pyrite, with values between 3.60 to 30.00%, obtaining the highest values for Landázuri-1 (see Tables 1 and 2). In the coal seams analyzed, the pyrite was characterized according to morphology into framboidal, granular, massive, and crystalline. It was observed replacing macerals and filling voids and fractures (Fig. 5b, 5g, 5h, 5i, 6b, 6j).

Correlations between macerals of Vitrinite and Inertinite groups, and the petrographic indexes (GI, TPI, VI, GWI, and Vitrinite- VI radius) are listed in Tables 3 and 4.

Group selection

The Elbow plots shown in Figures 8 A and B allows us to discriminate seams groups for each well. Three seams' groups from the Landázuri 1 well show that the quadratic distance between the elements that comprise them is less than 20,000. While Landázuri 2 well has a distance between two and three seams' groups in the range between 30,000 and 50,000. Although, for both wells with 4 and 5 groups, the distance is minimized the samples number within each was taken into account. The Landázuri 1 well consists of fourteen core samples, while the Landázuri 2 well comprises 11 samples. Accepting groups of 4 or 5 would imply that they would be formed by 1 or 2 samples and, in that case, the correlations between the variables would not make any geological sense, since any straight line could be adjusted by linear regression of two measurements. Thus, we decided to keep the 3 groups for Landázuri 1 and 2 groups for Landázuri 2 (Fig. 7). The dendograms produced using PCA (Principal Component Analysis) analysis suggest that the samples integrate each group according to the measured gas content (Fig. 8).

Linear regression analysis

Relationship between measured gas volume and Vitrinite Reflectance

The coal rank has been defined as an important factor in the maceral composition variation and, therefore, in the gas storage capacity (e.g., Crosdale et al. 1998, 2017; Keshavarz 2017). Other authors deduced that a higher coal rank indicates a greater depth, and as the Vitrinite percentage increases the gas content is higher (Bustin and Clarkson 1998, among others). In the Landázuri coals, the reflectance analysis reveals that the gas content does not increase proportionally with rank, nor with depth, taking into account that the highest reflectance values are not found in the lowest stratigraphic position (see Fig. 9 a,c).

It is evident that the middle-to-high range coals- (MVB- LVB) from the Landázuri 1 well, duplicate in gas content the lower-range coals (HVB - MVB) from the Landázuri 2 well. The gas content (< 600 SCF / ton- Landázuri 1 and <300- Landázuri 2) have no relationship with Vitrinite Reflectance, while the groups

with higher gas content present a correlation factor R2 = 0.74 for Landázuri 1 and 0.99 for Landázuri 2 (Fig. 9 b, d).

Relationship between measured gas volume and the Vitrinite Group

The relationship between the Vitrinite percentage and the gas content indicates as the Vitrinite content increases, the gas adsorption capacity decreases, showing a negative slope in the correlation graph (Hackley et al. 2000; Mares and Moore 2008). The above applies to the groups defined with the higher measured gas content (>600- Landázuri 1 and >300- Landázuri 2). The other groups show a positive correlation, which indicates that as the percentage of Vitrinite the measured gas content also increases. The coal rank inclusion suggests that the Vitrinite content does not influence gas adsorption in the BMV-BBV rank coals (Laxminarayana and Crosdale 1999). That is the case for the Landázuri coals, with > 600 SCF/ton and > 300 SCF/ton gas content, the opposing relationship occurs in lower gas content coals. (see Fig. 10 a, b).

The dependence between structured (Telovitrinite, Gelovitrinite), and degraded (Detrovitrinite) macerals defines the Vitrinite radius. Fig. 10 shows the correlation with positive character in the medium to high-rank Landázuri 1 coals with a gas content measured between 200-800 SCF/ton. The VR is irrelevant in <200 SCF / ton gas content coals because of its zero tendency. The coals of the Landázuri 2 well have a positive correlation with the gas content reflecting the Vitrinite structured macerals importance. (See Fig. 10 c, d; Tables 3 and 4).

Relation between measured gas content and the Inertinite Group

The correlation of the Inertinite percentage with the gas content suggests a positive influence in the groups with higher gas content (>600 and >300 SCF/ton). The remaining groups indicate a correlation with a negative trend. (See Fig. 11; Table 1 to 4).

The IR has merit in the defined coals groups, specifically in the >600 SCF/ton gas content -Landázuri 1, where the degraded Inertinite is higher than the structured Inertinite. (See Fig. 11a, b; Table 1 to 4).

The Inertinite cellular structure is an important factor in methane gas enrichment in the defined groups with higher gas content. It is contrary to what was observed with the percentage of Vitrinite with a high degree of metamorphism that does not allow filling the pores with gas. (e.g., Mares and Moore 2008; Wang 2018). Although an inverse relationship of the Inertinite radius is observed in the > 600 SCF/ton group, the pore size distribution and its role in the gas desorption process in both structured and the degraded inerts remain significant (see Fig. 11c, d).

Relationship between the measured gas content and the mineral matter percentage

The relationships between the mineral matter content with the measured gas content do not show correlation or tend to zero, except in the group <300 SCF/ton in Landázuri 2 (see Fig. 12). The pyrite is observed as euhedral and anhedral, framboidal grains or crystals, filling pores and voids, as an indicator of a syngenetic process (Raharjo 2018; Dai et al. 2020). The early syngenetic and diagenetic origin is related to a higher gas content in the coals of Landázuri 1. According to Bertrand (1989), this condition is due to the contribution of the microporosity of the mineral matter after the gelation process. The different forms of pyrite concentration are shown in Fig. 13. We discriminated that epigenetic pyrite concerns intermediate to low gas contents as occurs in coal seams: M17 and M2 in Landázuri 2, this reduction in methane gas sorption, according to Raharjo (2018) could be due to the large size and area covered by pyrite, which, according to Laxminarayana (1999), and Warwick et al. (2008) reduce gas sorption by a retention process.

Relationship between measured gas content and the coal facies

The calculated indices were: TPI- Tissue Preservation Index, GI- Gelation Index, VI- Vegetation Index, GWI- Groundwater Index, and V/I radius. They are the water table variations concerning organic matter preservation and are calculated as follows:

$$TPI = Telinite + Colotelinite + Semifusinite + Fusinite / Colodetrinte + Macrinite + Inertodetrinite$$

$$GI = Vitrinite + Macrinite / Semifusinite + Fusinite + Inertodetrinite$$

$$GWI = Gelinite + Corpogelinite + Minerals\ (clay, quartz) + Vitrodetrinite / Telinite + Telocolinite + Colodetrinite$$

$$VI = Colotelinite + Fusinite + Semifusinite + Suberinite + Resinite / Colodetrinite + Inertodetrinite + Alginite + Liptodetrinite + Sporinite + Cutinite$$

The index that reveals the degree of persistence of wet and dry conditions is the GI (see Fig. 14e, f); and the GWI and the Vitrinite/Inertinite ratio (V/I) represent the degree of gelation of the fabrics according to the water and pH contributions (see Fig. 14c, d, i, j). These indices show the same behavior as the percentage of Vitrinite concerning the gas content illustrated in Fig. 10a, b. The GI value exception is the Landázuri 2 well with >300 SCF/ton content, with a very low Telovitrinite and Colodetrinite content; therefore, the index acquires a high value. On the other hand, the TPI index as an indicator of the degree of humification of organic matter macerals (see Fig. 14a, b) and the VI index (see Fig. 14g, h) show the contrast of macerals of forest affinity with herbaceous marginal, indicating the same trend as that of the VR in Fig. 10c, d.

The Calder et al. (1991) and Diessel (1986) models indicate that the organic matter in Landázuri was transformed in a limnic environment (marshy or lacustrine continental basins) that fulfills the Vitrinite> Inertinite and Degraded Vitrinite> Structured Vitrinite condition (Fig. 15 and 16). The coal facies variation is not evident in the same geological formation, as the seams are from the same well.

Pearson's analysis

The relationships between pairs of variables are plotted as Pearson correlograms, these summarized the linear regression analysis, highlighting the inertinitic macerals contribution in the group of each well with higher desorbed gas content and of Vitrinite (V) and V/I radius in the coals categorized with medium to low

gas content (see Fig. 17). For these correlograms, only variables that have a relationship were plotted using a p-value of 0.25. Additionally, the correlograms allow us to corroborate other linear relationships between variables that had not been considered before and to identify their influence on the response variable, as is the case of gas content.

Multiple regression analysis

The analysis was performed considering the variable Gas V (Gas Volume) as the response variable and the variables: Ro, StrV, StrI, Gas V, %V, and %I as the predictor variables.

In Tables 5 and 6, a summary of the multiple linear regression statistics is presented for the initial and final models of the Landazuri-1 well. According to the Table 5 none of the five predictor variables (Ro, Str I, Str V, %V and %I) would be significant in the calculation of gas volume. The closest is Str V with a probability of 0.133. The adjusted regression coefficient is 0.05362 and p-value= 0.3984. Once the stepwise selection procedure is applied, Table 6 shows that the Str V variable is significant assuming a reliability level of 99%, the adjusted R2= 0.229 increases, while the p-value diminishes to 0.08328, which imply that the two predictors' variables Str I and Str V are significant to reproduce the gas volume.

Considering the same five predictor variables previously mentioned, in Table 7 we summarized the multiple linear regression results for the Landazuri-2 well. According to this Table, only Str V is a significant variable with a probability of 0.0998 for the gas volume estimation. However, Ro and Str I are other variables that could have a significant effect on gas volume, with probabilities of 0.2411 and 0.2235, respectively. After the application of the stepwise method adjusted R2 correlation coefficient shows an improvement with respect to the initial model, evolving from 0.6991 to 0.7508. Similarly, the p-value of the initial model improves from 0.04023 to 0.004795 in the final model. Thus, Ro, Str I, and Str V represent significant predictors assuming a confidence level of 99%. (see Table 8). Fig. 18 shows in blue those predictor variables that have a positive influence with the gas content. The analysis highlights the Reflectance Vitrinite importance and

461 the structured macerals content in the coal seams related to the gas content, which
462 is a consequence of the coal formation history.
463

464 Conclusions

465 The measured gas volumes (SCF/ton) in the rank HVBA- MVB Landázuri 2 coals
466 fluctuate between 37.54 to 484.8, while rank MVB- LVB Landázuri 1 coals
467 doubles it, reaching values of 818.14 SCF/ton. The definition of the groups
468 according to the measured gas content allows highlighting the relationship of the
469 maceral composition with the pore size (micropore, macropore, mesopore), and
470 the coal rank.
471
472 The petrographic variables analyzed to reveal that the groups with the highest gas
473 content (> 600 SCF / ton- MVB, LVB-Landázuri 1;> 300 SCF / ton- HVBA,
474 MVB-Landázuri 2) exhibit higher content of inertinite (macropore, mesopore),
475 while the medium to low gas content is directly related to the content of vitrinite
476 (micropore) emphasizing structured macerals (see Fig. 19).
477
478 Further, mineral matter contributes microporosity about gas content showing
479 positive correlation except in coals >300 SCF/ton from Landázuri 2. The pyrite
480 syngenetic and early diagenetic is related to higher gas content, while epigenetic
481 pyrite concentration covers the greater surface area and is related to intermediate
482 to low measured gas contents.
483
484 The maceral relationship in the definition of the petrographic indices reveals
485 limnic facies of continental swampy or lacustrine basins. The GI, GWI, and V/I
486 indices present the same behavior as the Vitrinite content in each group analyzed,
487 except for the high GI value in the group with >300 in Landázuri 2 well, as the
488 result of the low Telovitrinite and Colodetrinite content. The TPI and VI indices
489 are equivalent to the Vitrinite radius.
490

491 Acknowledgments

The authors would like to thank the geological engineers Claudia Duarte, Luis Fernando Ortiz, Fernando Andres Parra of the Energetics Group - Servicio Geológico Colombiano, for the detailed field work, drilling and desorption analysis of the coal seams; the group of professionals of the Laboratory of Characterization, Processing and Research of Coal and Energetic Materials - Servicio Geológico Colombiano, for the reflectance analysis of the selected samples. Mauricio Bermúdez thanks the UPTC SGI-DIN-3104 Project.

Declarations

Funding This research is part of the Exploration in Energy Resources Project of the Servicio Geológico Colombiano.

Availability of data and materials Applicable.

Conflict of interest: The authors have no conflicts of interest to declare that are relevant to the content of this article.

References

ASTM. (2005). D2799-05 "Standard test method for microscopical determination of the maceral composition of coal" ASTM Philadelphia

ASTM (2005b) D2798–05 Standard test method for microscopical determination of the vitrinite reflectance of coal. ASTM Philadelphia

Bertrand, P. R. (1989). Microfacies and petroleum properties of coals as revealed by a study of North Sea Jurassic coals. 13, 575–595.

Blandón, A. (2007). Contribución de la materia orgánica sedimentaria a la determinación del paleoambiente y del potencial de generación de hidrocarburos en los carbones de la Formación Amagá (Colombia). These de doctorat: Univ. Genève 2006 no. Sc. 3806

BP (2021) BP statistical review of world energy 2020 70th edition. BP plc London. https://www.bp.com/content/dam/bp/business-sites/en/global/corporate/pdfs/energy-economics/statistical-review/bp-stats-review-2021-full-report.pdf

Busch, A., & Gensterblum, Y. (2011). CBM and CO2-ECBM related sorption processes in coal: A review. International Journal of Coal Geology, 87(2), 49–71. https://doi.org/10.1016/j.coal.2011.04.011

Busch, A., Han, F., y Magill, C. R. (2019). Paleofloral dependence of coal methane sorption capacity. International Journal of Coal Geology, 211(June). https://doi.org/10.1016/j.coal.2019.103232

Bustin, A. M. M., y Bustin, R. M. (2016). Total gas-in-place, gas composition and reservoir properties of coal of the Mannville coal measures, Central Alberta. International Journal of Coal Geology, 153, 127–143. https://doi.org/10.1016/j.coal.2015.11.011

Bustin, R. M., & Clarkson, C. R. (1998). Geological controls on coalbed methane reservoir capacity and gas content. International Journal of Coal Geology, 38(1–2), 3–26. https://doi.org/10.1016/S0166-5162(98)00030-5

Calder, J. H., Gibling, M. R., y Mukhopadhyay, P. K. (1991). Peat formation in a Westphalian B piedmont setting, Cumberland Basin, Nova Scotia: implications for the maceral-based interpretation of rheotrophic and raised paleomires. Bulletin - Societe Geologique de France, 162(2), 283–298.

Cardott, B. J., y Curtis, M. E. (2018). Identification and nanoporosity of macerals in coal by scanning electron microscopy. International Journal of Coal Geology, 190(February 2017), 205–217. https://doi.org/10.1016/j.coal.2017.07.003

Castaño, L; Gómez, O. (2001). Caracterización, origen, evolución y potencial de utilización de los carbones de la Secuencia
Volcanoclástica de Aranzazu Caldas. Universidad de Caldas, Thesis

Chalmers, G. R. L., y Marc Bustin, R. (2007). On the effects of petrographic composition on coalbed methane sorption. International Journal of Coal Geology, 69(4), 288–304. https://doi.org/10.1016/j.coal.2006.06.002

Crosdale, P. J., Beamish, B. B., y Valix, M. (1998). Coalbed methane sorption related to coal composition. International Journal of Coal Geology, 35(1–4), 147–158. https://doi.org/10.1016/S0166-5162(97)00015-3

Crosdale, P. J. (2017). Coal bed methane. Geology: current and future developments. Eds. Suárez-Ruíz, I., Mendonça, João. Vol 1. 258-286

Dai S, Bechtel A, Eble CF et al (2020) Recognition of peat depositional environments in coal: a review. Int J Coal Geol
219:103383. https://doi.org/10.1016/j.coal.2019.103383

572 Diessel CFK. (1986). On the correlation between coal facies and depositional environments.
573 Proceeding of 20th symposium Department of Geology. University Newcastle NSW, 19– 22
574
575 Etayo-Serna, Fernando. 2019. "Basin development and tectonic history of the Middle Magdalena
576 Valley". En Estudios geológicos y paleontológicos sobre el Cretácico en la región del embalse del
577 río Sogamoso, Valle Medio del Magdalena, dirección científica y edición de Fernando Etayo-
578 Serna. Compilación de los Estudios Geológicos Oficiales en Colombia vol. XXIII. Bogotá:
579 Servicio Geológico Colombiano.
580
581 Gómez, L.A., Patiño, A., Renzoni, G., Beltrán, A., Quintero, C. y Manrique, M. (2008).
582 Cartografía geológica y muestreo geoquímico escala 1:100 000 de la plancha 119 Barrancabermeja
583 VMM. INGEOMINAS y GRP Ltda. Bogotá.
584
585 Gómez, J. S., López, M. D., 2017. Paleoenvironments of coals using organic petrography and their
586 relationship with physicochemical properties, Guaduas Formation, Checua-Lenguazaque syncline.
587 Tesis de grado- UPTC- Colciencias, Tunja
588
589 Guatame C, Sarmiento Perez G (2004) Interpretación del Ambiente Sedimentario de los Carbones
590 de la Formación Guaduas en el Sinclinal Checua-Lenguazaque a partir del análisis petrográfico.
591 Geología Colombiana 29:41–58
592
593 Guatame, C., & Rincón, M. (2021). Coal petrology analysis and implications in depositional
594 environments from upper Cretaceous to Miocene: a study case in the Eastern Cordillera of
595 Colombia. International Journal of Coal Science and Technology. https://doi.org/10.1007/s40789-
596 020-00396-z
597
598 Guo Q, Littke R., Zieger, L. (2018). Petrographical and geochemical characterization of sub-
599 bituminous coals from mines in the Cesar-Ranchería Basin, Colombia. Int J Coal Geol 191:66–79.
600 https://doi.org/10.1016/j.coal.2018.03.008
601 Hackley, P. C., Warwick, P. D., & Breland, F. C. (2007). Organic petrology and coalbed gas
602 content, Wilcox Group (Paleocene-Eocene), northern Louisiana. International Journal of Coal
603 Geology, 71(1 SPEC. ISS.), 54–71. https://doi.org/10.1016/j.coal.2006.05.009
604
605 Hartigan, J. A., & Wong, M. A., 1979. "A K-Means Clustering Algorithm." Applied Statistics 28:
606 100–108
607
608 Hou, H., Shao, L., Li, Y., Li, Z., Wang, S., Zhang, W., y Wang, X. (2017). Influence of coal
609 petrology on methane adsorption capacity of the Middle Jurassic coal in the Yuqia Coalfield,
610 northern Qaidam Basin, China. Journal of Petroleum Science and Engineering, 149(February),
611 218–227. https://doi.org/10.1016/j.petrol.2016.10.026
612

https://terrasolid.com/product/tgas/

ICCP. (1998). The new vitrinite classification (ICCP System 1994) Fuel, 77, 349-358

ICCP. (2001). The new inertinite classification (ICCP System 1994). Fuel, 80, 459-471

ISO (2014). 17892-2. Geotechnical investigation and testing — Laboratory testing of soil — Part 2: Determination of bulk density

Jian, K., Fu, X., Ding, Y., Wang, H., y Li, T. (2015). Characteristics of pores and methane adsorption of low-rank coal in China. Journal of Natural Gas Science and Engineering, 27, 207–218. https://doi.org/10.1016/j.jngse.2015.08.052

Kalkreuth, W. D., Marchioni, D. L., Calder, J. H., Lamberson, M. N., Naylor, R. D., & Paul, J. (1991). The relationship between coal petrography and depositional environments from selected coal basins in Canada. International Journal of Coal Geology, 19(1–4), 21–76. https://doi.org/10.1016/0166-5162(91)90014-A

Kendall, M. G., Stuart, A., 1973. The Advanced Theory of Statistics, Volume 2: Inference and Relationship, Griffin. ISBN 0-85264-215-6

Keshavarz, A., Sakurovs, R., Grigore, M., & Sayyafzadeh, M. (2017). Effect of maceral composition and coal rank on gas diffusion in Australian coals. International Journal of Coal Geology, 173, 65–75. https://doi.org/10.1016/j.coal.2017.02.005

Lamberson, M. N., y Bustin, R. M. (1993). Coalbed methane characteristics of Gates Formation coals, northeastern British Columbia: effect of maceral composition. In American Association of Petroleum Geologists Bulletin (Vol. 77, Issue 12, pp. 2062–2076). https://doi.org/10.1306/bdff8fd8-1718-11d7-8645000102c1865d

Laxminarayana, C., y Crosdale, P. J. (1999). Role of coal type and rank on methane sorption characteristics of Bowen Basin, Australia coals. International Journal of Coal Geology, 40(4), 309–325. https://doi.org/10.1016/S0166-5162(99)00005-1

Li, X., Fu, X., Liu, A., An, H., Wang, G., Yang, X., Wang, L., & Wang, H. (2016). Methane Adsorption Characteristics and Adsorbed Gas Content of Low-Rank Coal in China. Energy and Fuels, 30(5), 3840–3848. https://doi.org/10.1021/acs.energyfuels.6b00071

Lloyd, S., 1982. “Least Squares Quantization in Pcm.” IEEE Transactions on Information Theory 28 (2): 129–37

Li, S., Tang, D., Pan, Z., y Xu, H. (2014). Influence and control of coal facies on physical properties of the coal reservoirs in Western Guizhou and Eastern Yunnan, China. International Journal of Oil, Gas and Coal Technology, 8(2), 221–234. https://doi.org/10.1504/IJOGCT.2014.064837

Li, Y., Cao, D., Wu, P., Niu, X., y Zhang, Y. (2017). Variation in maceral composition and gas content with vitrinite reflectance in bituminous coal of the eastern Ordos basin, China. Journal of Petroleum Science and Engineering, 149(August), 114–125. https://doi.org/10.1016/j.petrol.2016.10.018

Mares, T. E., y Moore, T. A. (2008). The influence of macroscopic texture on biogenically-derived coalbed methane, Huntly coalfield, New Zealand. International Journal of Coal Geology, 76(1–2), 175–185. https://doi.org/10.1016/j.coal.2008.05.013

Mariño-Martínez, J. E., & Mojica-Amaya, A. (2014). Relación entre la petrografía del carbón y el contenido de gases en la cuenca de Amagá (Antioquia, Colombia). Revista Facultad De Ingeniería, 23(37), 33. https://doi.org/10.19053/01211129.2788

Mariño, J.E., Castro-Rodríguez, A., Botero, .A, Mojica, L., Granados, D., Acuña, C. (2015). GAS ASOCIADO AL CARBÓN (CBM o GMAC), Geología, contenidos, reservas, mineria y posibilidades en Colombia. ISBN: 978-958-660-212-9

Mastalerz, M., y Drobniak, A. (2020). Coalbed methane: Reserves, production, and future outlook. In Future Energy: Improved, Sustainable and Clean Options for Our Planet. Elsevier Ltd. https://doi.org/10.1016/B978-0-08-102886-5.00005-0

Mejía L.J; Convers C.E; González J.F. (2006). Coal microlithotype analysis of the Guaduas Formation in the Sueva Syncline, Cundinamarca, Colombia. Geología Colombiana 31:11–26

MONROY, W., SANDOVAL, M. 2014. Exploración y Evaluación de carbones en el Área Cimitarra Sur y sur del Área Río Opón-Landázuri del Departamento de Santander. Servicio Geológico Colombiano. Bogotá.

Moore, T. A. (2012). Coalbed methane: A review. International Journal of Coal Geology, 101, 36–81. https://doi.org/10.1016/j.coal.2012.05.011

Ortiz, L., Parra, F., Duarte., y Rincón, M. (2016). Exploración gas metano asociado al carbón. Área Landázuri – Velez. Departamento de Santander. Bogotá: Servicio Geológico Colombiano

Pickel W, Kus J, Flores D et al (2017) Classification of liptinite – ICCP System 1994. Int J Coal Geol 169:40–61. https://doi.org/10.1016/j.coal.2016.11.004

Raharjo, S., Bahagiarti, S., Purwanto, H. S., y Rahmad, B. (2018). The effect of coal petrology on the capacity of gas methane absorption in coal formation Tanjung Barito in Binuang Region, South Kalimantan. IOP Conference Series: Earth and Environmental Science, 212(1). https://doi.org/10.1088/1755-1315/212/1/012029

Sarmiento, G., Puentes, J., & Sierra, C. (2015). Evolución geológica y estratigrafía del sector norte del Valle Medio del Magdalena. Geologia Norandina, 12, 51–83. http://sociedadcolombianadegeologia.org/wp-content/uploads/2017/06/Norandina_No.12_Art4.pdf

Schwarz, G., 1978, Estimating the Dimension of a Model: Annals of Statistics, v. 6, p. 461-464.

Singh, A. K. (2016). Petrographic characterization and evolution of the Karharbari coals, Talcher Coalfield, Orissa, India. International Journal of Coal Science and Technology, 3(2), 133–147. https://doi.org/10.1007/s40789-016-0132-3

Suárez-Ruiz, I., Flores, D., Mendonça Filho, J. G., & Hackley, P. C. (2012). Review and update of the applications of organic petrology: Part 1, geological applications. International Journal of Coal Geology, 99, 54–112. https://doi.org/10.1016/j.coal.2012.02.004

Terraza Melo, Roberto. 2019. "'Formación La Luna': expresión espuria en la geología colombiana". En Estudios geológicos y paleontológicos sobre el Cretácico en la region del embalse del río Sogamoso, Valle Medio del Magdalena, dirección científica y edición de Fernando Etayo-Serna. Compilación de los Estudios Geológicos Oficiales en Colombia vol. XXIII. Bogotá: Servicio Geológico Colombiano

Wang, K., Fu, X., Qin, Y., y Sesay, S. K. (2011). Adsorption characteristics of lignite in China. Journal of Earth Science, 22(3), 371–376. https://doi.org/10.1007/s12583-011-0189-2

Wang, M. S., Zou, G. G., y Zhu, R. B. (2018). Relationship between Maceral of Coal and Coal-bed Methane adsorption ability in Sihe Coalmine of Qinshui Basin, China. IOP Conference Series: Materials Science and Engineering, 359(1), 0–6. https://doi.org/10.1088/1757-899X/359/1/012026

Warwick, P. D., Breland, F. C., & Hackley, P. C. (2008). Biogenic origin of coalbed gas in the northern Gulf of Mexico Coastal Plain, U.S.A. International Journal of Coal Geology, 76(1–2), 119–137. https://doi.org/10.1016/j.coal.2008.05.009

FIGURES CAPTIONS

Fig. 1 Geological map of the Landázuri- Vélez area- Middle Magdalena Valley Basin. Source: (Ortíz et al. 2016)

Fig. 2 Generalized stratigraphic column of the Upper Cretaceous- Middle Magdalena Valley Basin and Coal seams distribution from Landázuri 1 and 2 wells. Source: (Ortíz et al. 2016; Etayo-Serna 2019)

Fig. 3 Gas desorption curve (Ortíz et al. 2016)

Fig. 4 Ash-free gas content (SCF/ton) of coal seams from Landázuri 1 and Landázuri 2 wells (Ortíz et al. 2016)

Fig. 5 Coal seams photomicrographs of the Landázuri 1 well after desorption gas process. a. Clay filling inert´s empty spaces -M23, b. Framboidal pyrite -M21, c. Devolatized Colodetrinite -M20, d. Clay mineral matter -M17, e. Fractured Vitrinite and structured Fusinite -M14, f. Inertodetrinite in devolatized Colodetrinite -M13, g. Framboidal pyrite in Semifusinite -M12, h. Mineral matter -M11, i. Pyrite -M10, j. Vitrodetrinite, k. Colodetrinite -M7, l. Devolatized Vitrinite -M6, m. Preserved Fusinite and Inertodetrinite- M5, n. Vitrinite and inerts after desorption -M4, o. Degraded inerts - M3

Fig. 6 Coal seams photomicrographs of the Landázuri 2 well after desorption gas process. a. Clay minerals -M18, b. Pyrite filling Inertinite´s spaces -M17, c. Devolatilized Vitrinite - M16, d. Clay minerals in fractured Vitrinite -M15, e. Colotelinite and Vitrodetrinite -M14, f. Inert in Colodetrinite -M11, g. Semifusinite´s spaces filled with mineral matter -M10, h. Empty spaces in Colodetrinite and Semifusinite - M9, i. Inertodetrinite in Colodetrinite -M5, j. Pyrite in Fusinite -M3, k. Fusinite -M2

Fig. 7 Elbow-plots for (A) Landázuri 1and (B) Landázuri 2 wells

Fig. 8 Dendograms showing results of cluster analysis (A) Landázuri-1 (B) Landázuri-2 wells

Fig. 9 Coal rank (Ro) relation with depth and gas content measured (%Ro) (a, c) Landázuri-1 well. (b,d) Landázuri-2 well

HVBA- High Volatile Bituminous A, MVB- Medium Volatile Bituminous, - LVB Low Volatile Bituminous.

Fig. 10 Relationship between Vitrinite percentage (fmmb) and the Vitrinite Radius with the gas content (SCF/ton) (a, c) Landázuri-1 well, (b,d) Landázuri-2 well

Fig. 11 Relationship between Inertinite content (fmmb) and the Inertinite Radius with the gas content (scf/ton) (a, c) Landázuri-1 well, (b, d) Landázuri-2 well

Fig. 12 Relationship between mineral matter and the gas content (SCF/ton) (A). Landázuri 1 (B) Landázuri 2

Fig. 13 Microphotographs a. Clay minerals in M5- Landázuri-1, b. Clay minerals and pyrite -M17- Landázuri-2, c. Clay and others -M21- Landázuri-1, d. Framboidal pyrite -M17- Landázuri-2, e. Framboidal pyrite -M17-Landázuri-2, f. Framboidal pyrite -M7-Landázuri-1, g. Framboidal pyrite -M7-Landázuri-2, h. Syngenetic-diagenetic pyrite -M3-Landázuri-2, i. Epigenetic pyrite -M17-Landázuri-2, j. Epigenetic pyrite -M2-Landázuri-2, k. Epigenetic pyrite -M17-Landázuri-2, l. Syngenetic framboidal pyrite -M16-Landázuri-2, m. Diagenetic pyrite -M17-Landázuri-1, n. Diagenetic pyrite -M4-Landázuri-1, o. Diagenetic pyrite -M10-Landázuri-1, p. Late diagenetic pyrite? -M17-Landázuri-2

Fig. 14 Relationships between gas content (SCF/ton) and petrographic indexes (TPI, GWI, GI, VI, and V/I)

Fig. 15 Coal facies (GI, TPI) Source: Diessel (1986) and modified by Kalkreuth et al. 1991. a. Landázuri 1. b. Landázuri 2 A. Vitrinite> Inertinite, Degraded Vitrinite> Structured Vitrinite B. Vitrinite> Structured Inertinite, Vitrinite> Degraded Vitrinite C. Inertinite> Vitrinite Inertodetrinite> Semifusinite- Fusinite D. Inertinite> Vitrinite Semifusinite+Fusinite> Inertodetrinite

Fig. 16 Coal facies (GWI, VI). a. Landázuri 1 b. Landázuri 2 (Modified from Calder et al. 1991)

Fig. 17 Pearson correlograms showing relationships between pairs of variables for Landázuri 1 and Landázuri-2

Ro- Average Vitrinite Reflectance, V fmmb - Vitrinite free mineral matter, I fmmb- Inertinite free mineral matter, mm- mineral matter, V/I- Vitrinite/Inertinite radius, Deg V- Degraded Vitrinite, Str I - Structured Inertinite, Deg I - Degraded Inertinite, Str V- Structured Vitrinite, RV- Vitrinite Radius, IR- Inertinite Radius, Gas V- Total gas volume measured SCF/ton

Fig. 18 Behavior analysis of predictor variables (Str V, Str I, %V, %I, Ro) versus response variable (Gas V) for the wells: a. Landazuri 1 and b. Landazuri 2

Fig. 19 Synthesis of the importance of maceral groups and reflectance for the measured gas content

TABLES CAPTIONS

Table 1. Mean Vitrinite reflectance, measured gas volume, and maceral composition of the coal seams - Landázuri 1 well

Table 2. Mean Vitrinite reflectance, measured gas volume, and maceral composition of the coal seams- Landázuri 2 well

Table 3. Relationships between maceral content and petrographic indexes for coal seams of the Landázuri 1 well

Table 4. Relationships between maceral content and petrographic indexes for coal seams of the Landázuri 2 well

Table 5. Summary of multiple linear regression for initial model of the Landazuri-1 well

Table 6. Summary of multiple linear regression for final model of the Landazuri-1 well

Table 7. Summary of multiple linear regression for initial models of the Landazuri-2 well

Table 8. Summary of multiple linear regression for final model of the Landazuri-2 well

Figures

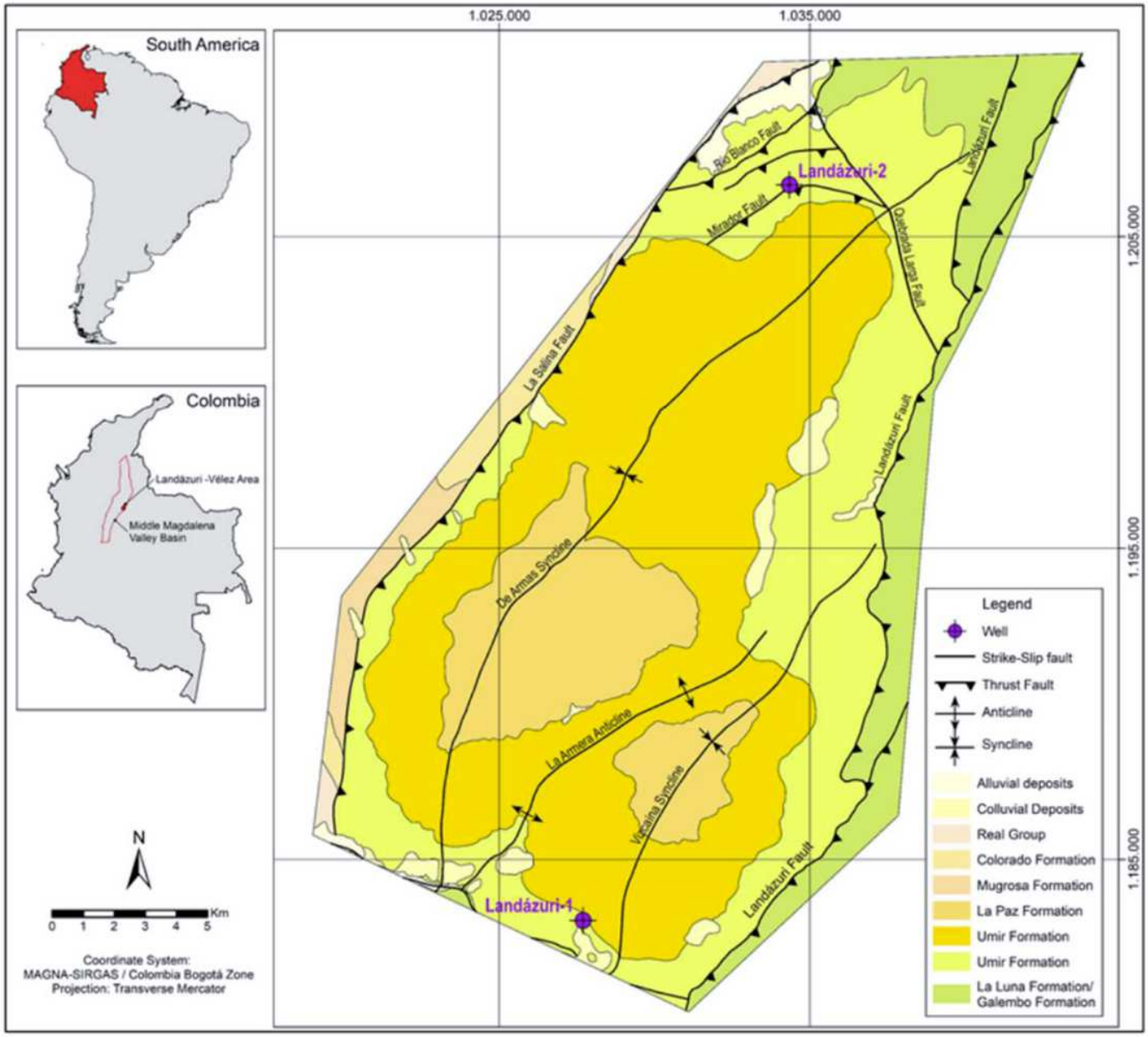

Figure 1

Geological map of the Landázuri- Vélez area- Middle Magdalena Valley Basin. Source: (Ortíz et al., 2016)

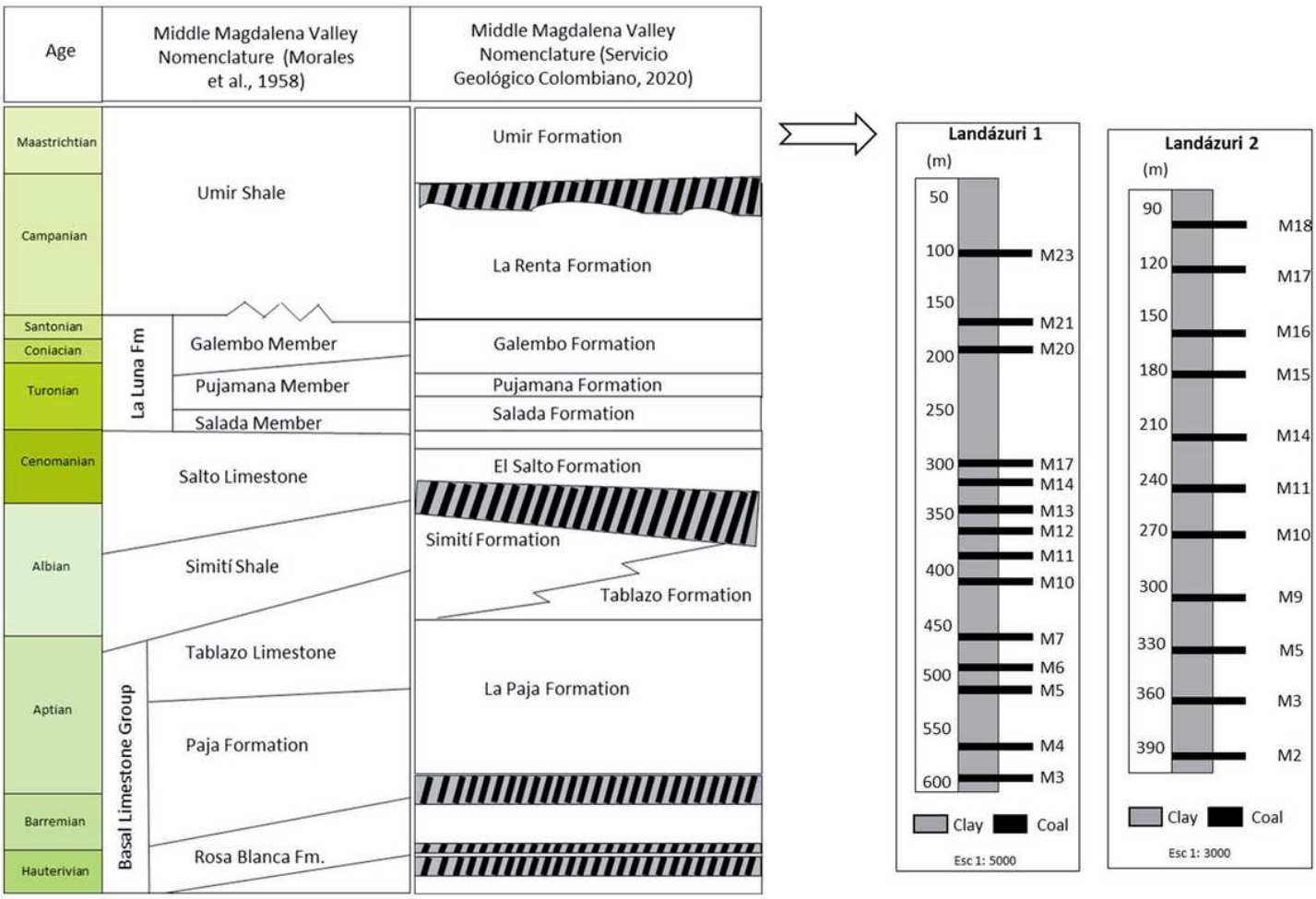

Figure 2

Generalized stratigraphic column of the Upper Cretaceous- Middle Magdalena Valley Basin and Coal seams distribution from Landázuri 1 and 2 wells. Source: (Ortíz et al., 2016; Etayo-Serna, 2019)

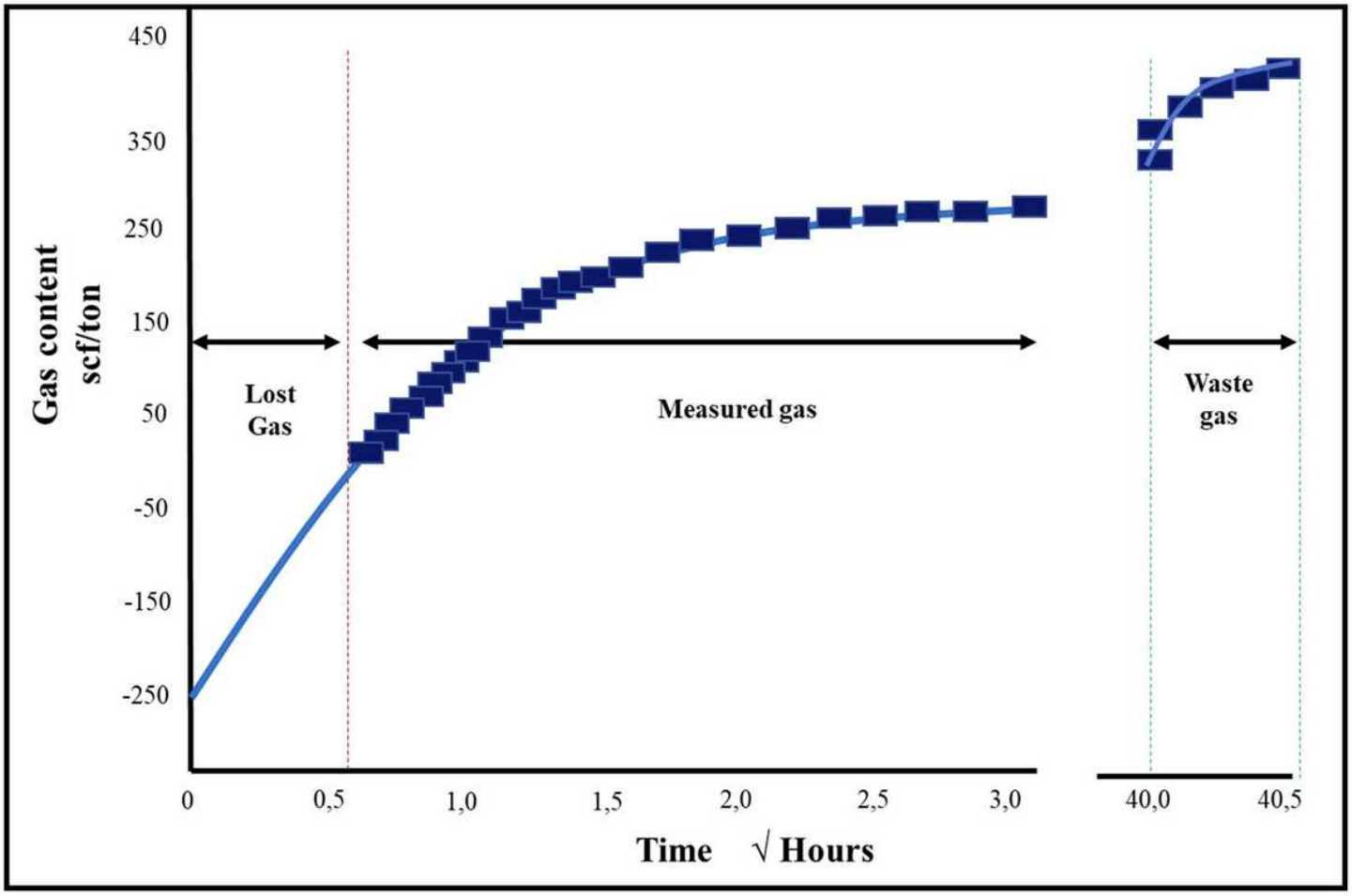

Figure 3

Gas desorption curve (Ortíz et al., 2016)

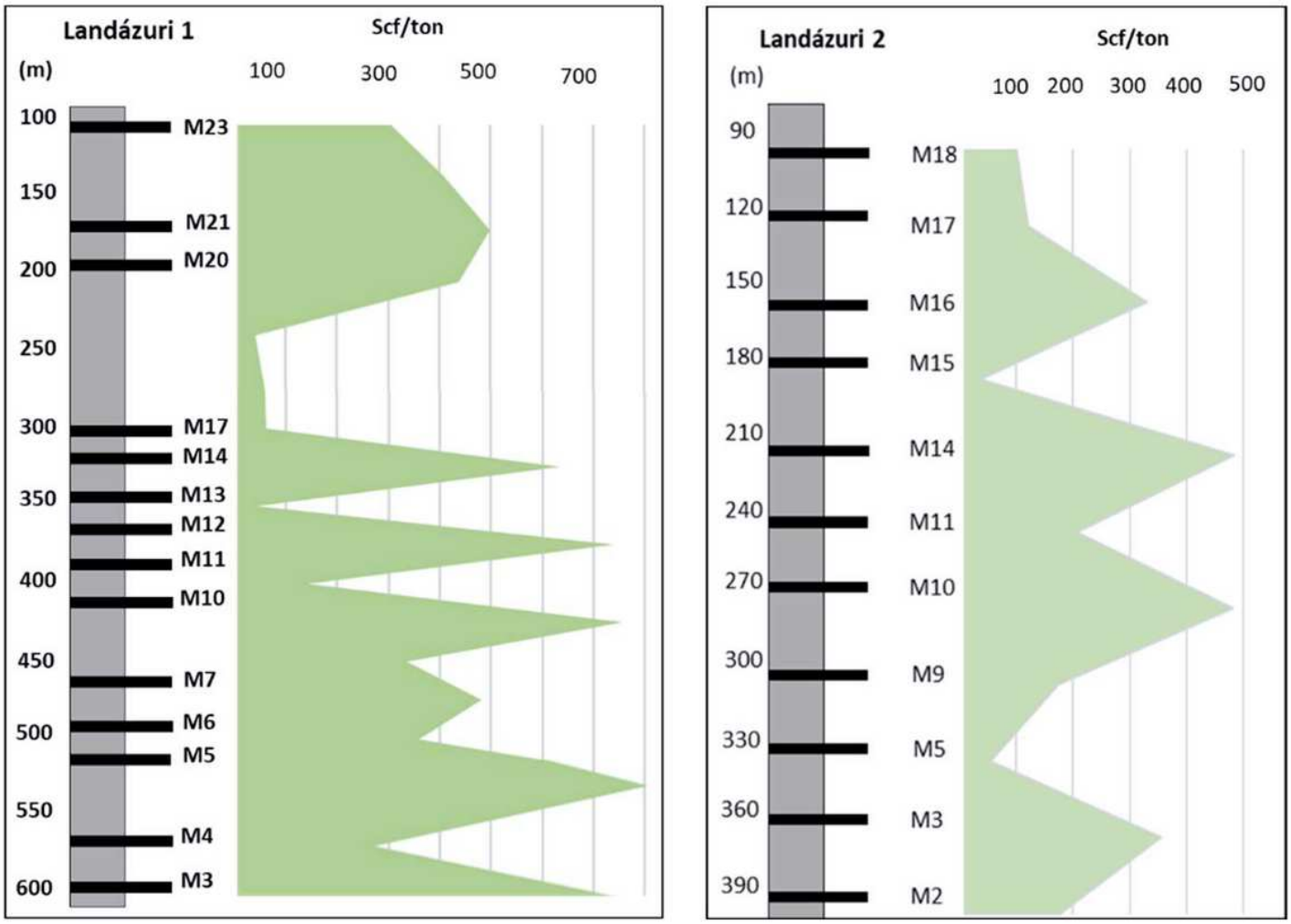

Figure 4

Ash-free gas content (SCF/ton) of coal seams from Landázuri 1 and Landázuri 2 wells (Ortíz et al., 2016)

Figure 5

Coal seams photomicrographs of the Landázuri 1 well after desorption gas process. a. Clay filling inert´s empty spaces -M23, b. Framboidal pyrite -M21, c. Devolatized Colodetrinite -M20, d. Clay mineral matter -M17, e. Fractured Vitrinite and structured Fusinite -M14, f. Inertodetrinite in devolatized Colodetrinite -M13, g. Framboidal pyrite in Semifusinite -M12, h. Mineral matter -M11, i. Pyrite -M10, j. Vitrodetrinite, k. Colodetrinite -M7, l. Devolatized Vitrinite -M6, m. Preserved Fusinite and Inertodetrinite- M5, n. Vitrinite and inerts after desorption -M4, o. Degraded inerts - M3

Figure 6

Coal seams photomicrographs of the Landázuri 2 well after desorption gas process. a. Clay minerals - M18, b. Pyrite filling Inertinite´s spaces -M17, c. Devolatilized Vitrinite - M16, d. Clay minerals in fractured Vitrinite -M15, e. Colotelinite and Vitrodetrinite -M14, f. Inert in Colodetrinite -M11, g. Semifusinite´s spaces filled with mineral matter -M10, h. Empty spaces in Colodetrinite and Semifusinite - M9, i. Inertodetrinite in Colodetrinite -M5, j. Pyrite in Fusinite -M3, k. Fusinite - M2

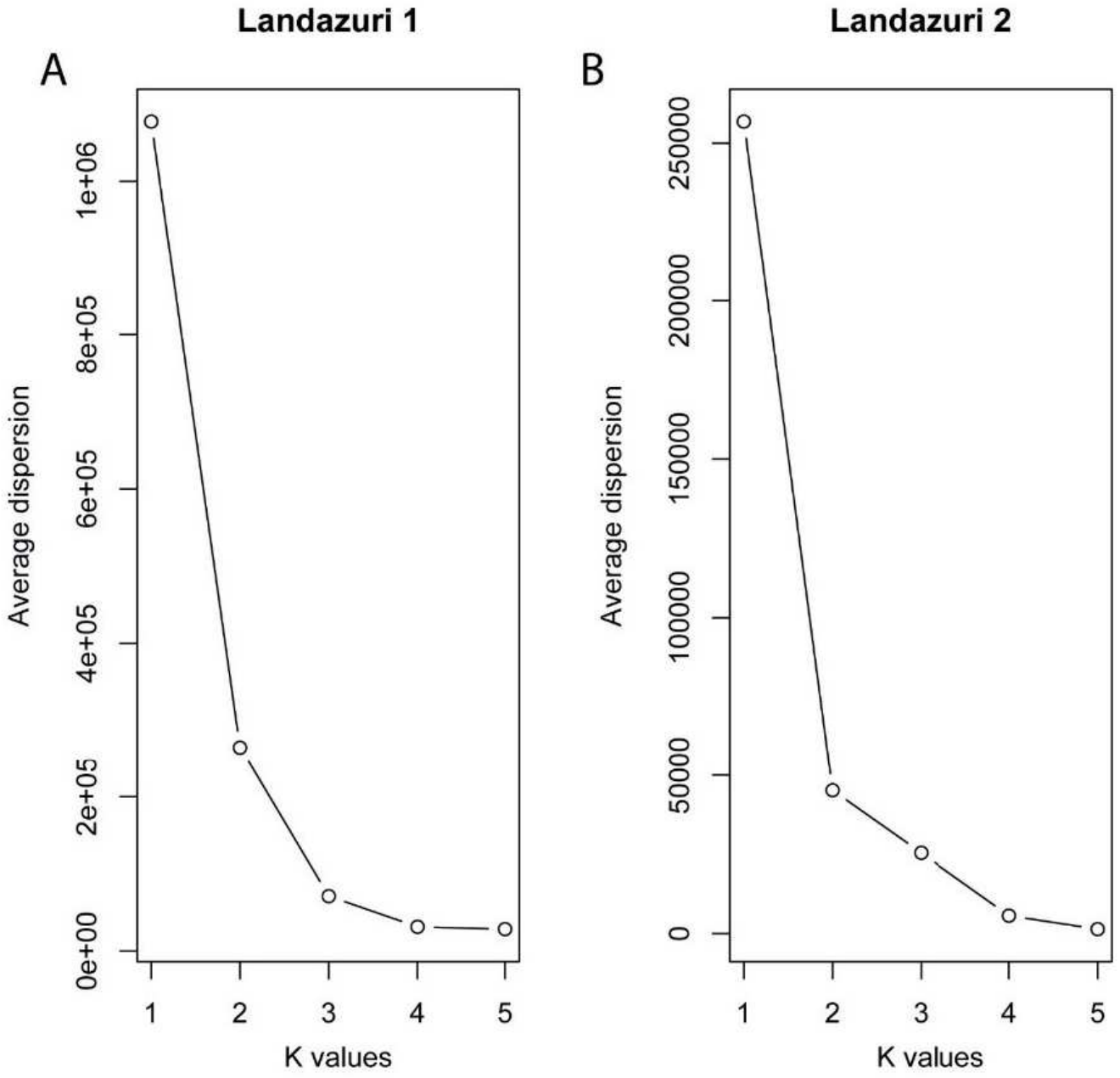

Figure 7

Elbow-plots for (A) Landázuri 1and (B) Landázuri 2 wells

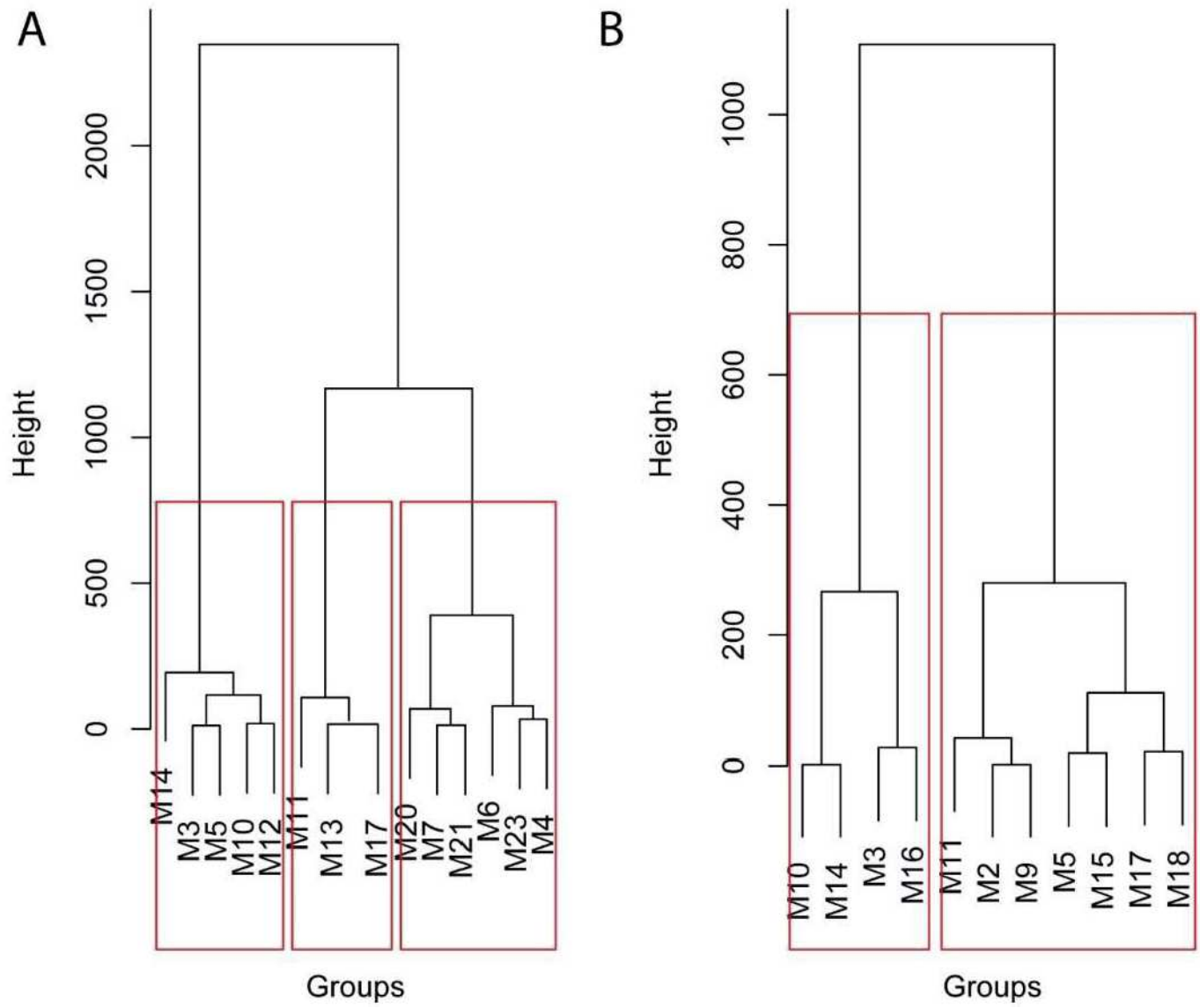

Figure 8

Dendograms showing results of cluster analysis (A) Landázuri-1 (B) Landázuri-2 wells

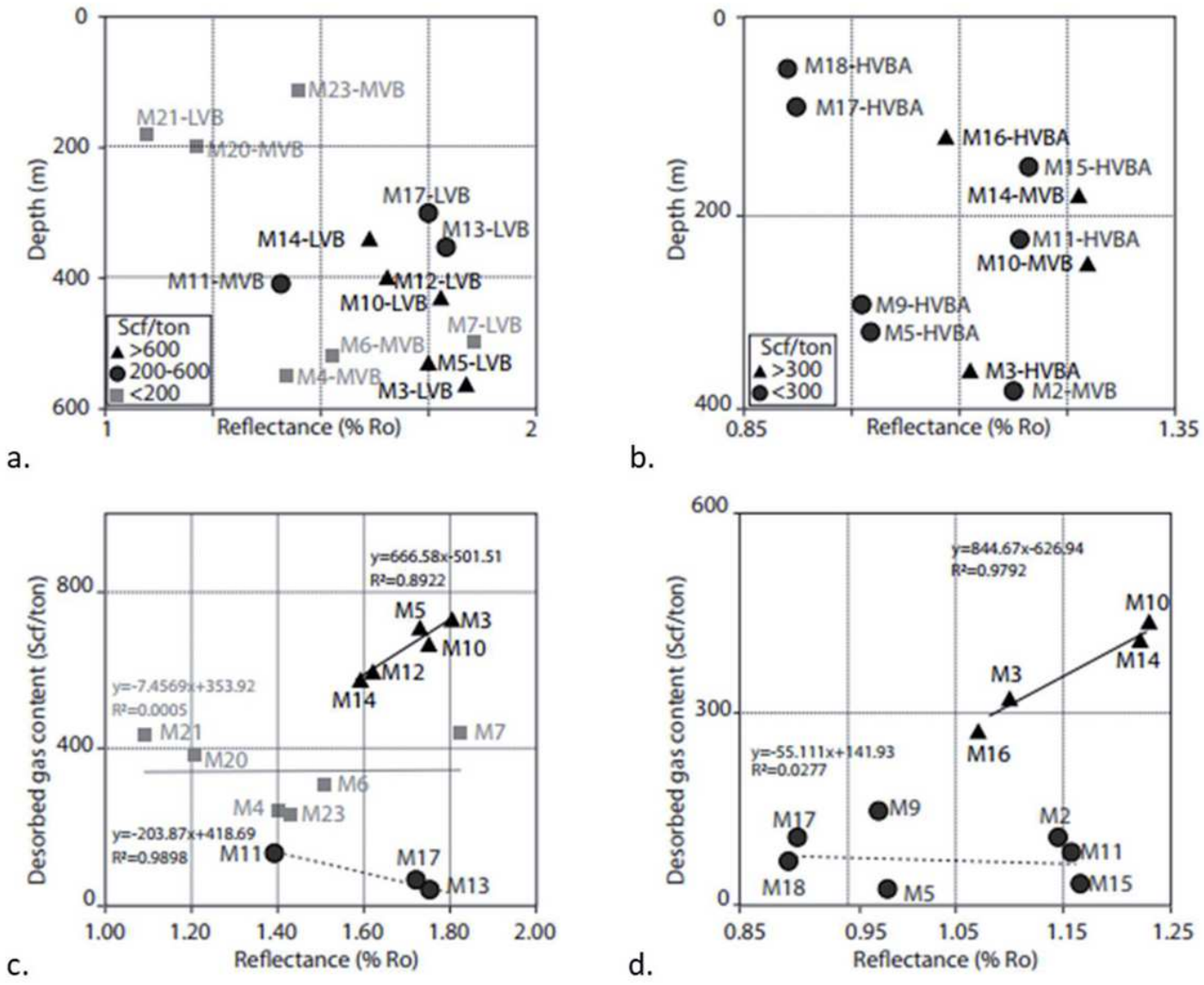

Figure 9

Coal rank (Ro) relation with depth and gas content measured (%Ro) (a, c) Landázuri-1 well. (b,d) Landázuri-2 well. HVBA- High Volatile Bituminous A, MVB- Medium Volatile Bituminous, - LVB Low Volatile Bituminous

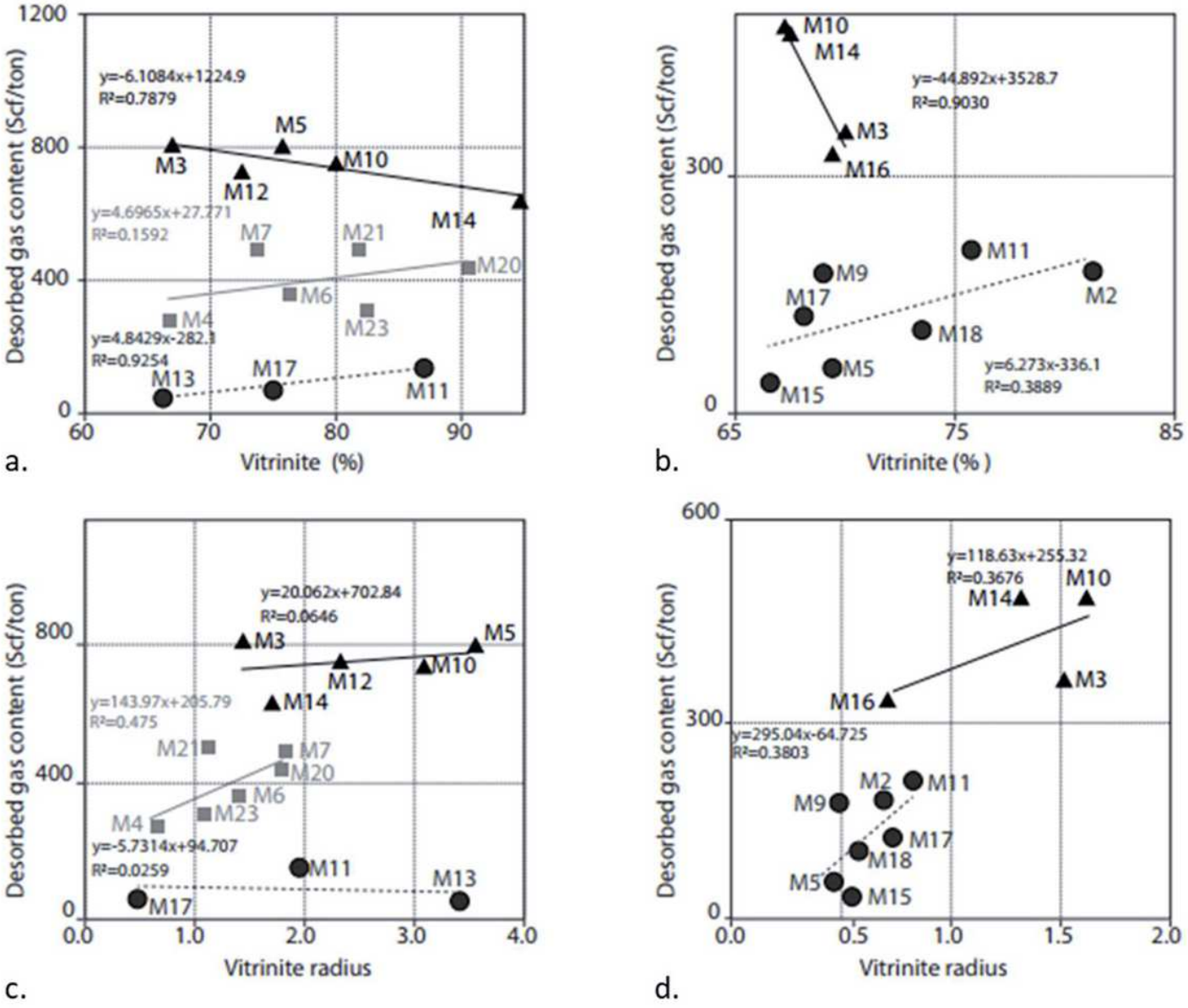

Figure 10

Relationship between Vitrinite percentage (fmmb) and the Vitrinite Radius with the gas content (SCF/ton) (a, c) Landázuri-1 well, (b,d) Landázuri-2 well

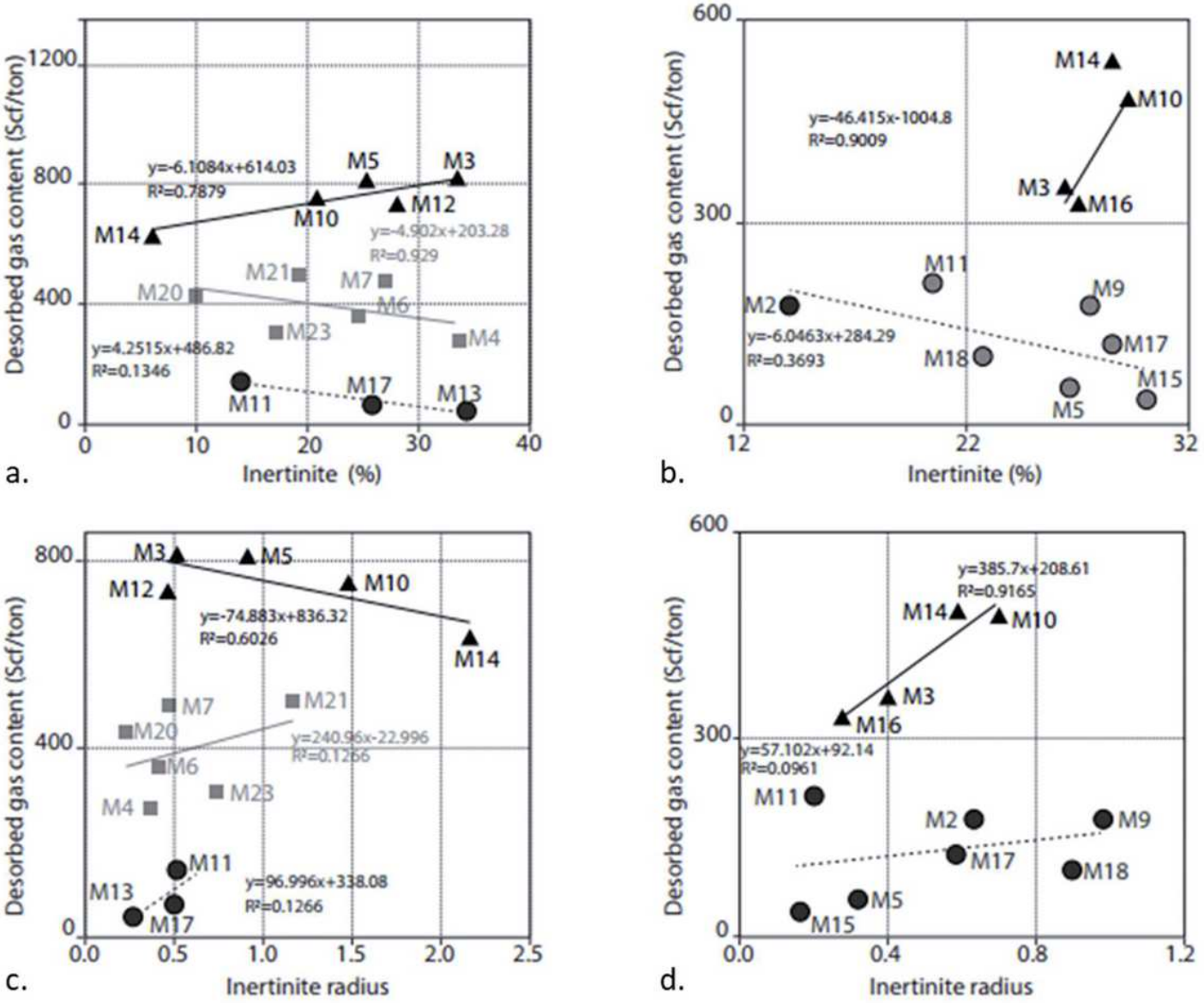

Figure 11

Relationship between Inertinite content (fmmb) and the Inertinite Radius with the gas content (scf/ton) (a, c) Landázuri-1 well, (b, d) Landázuri-2 well

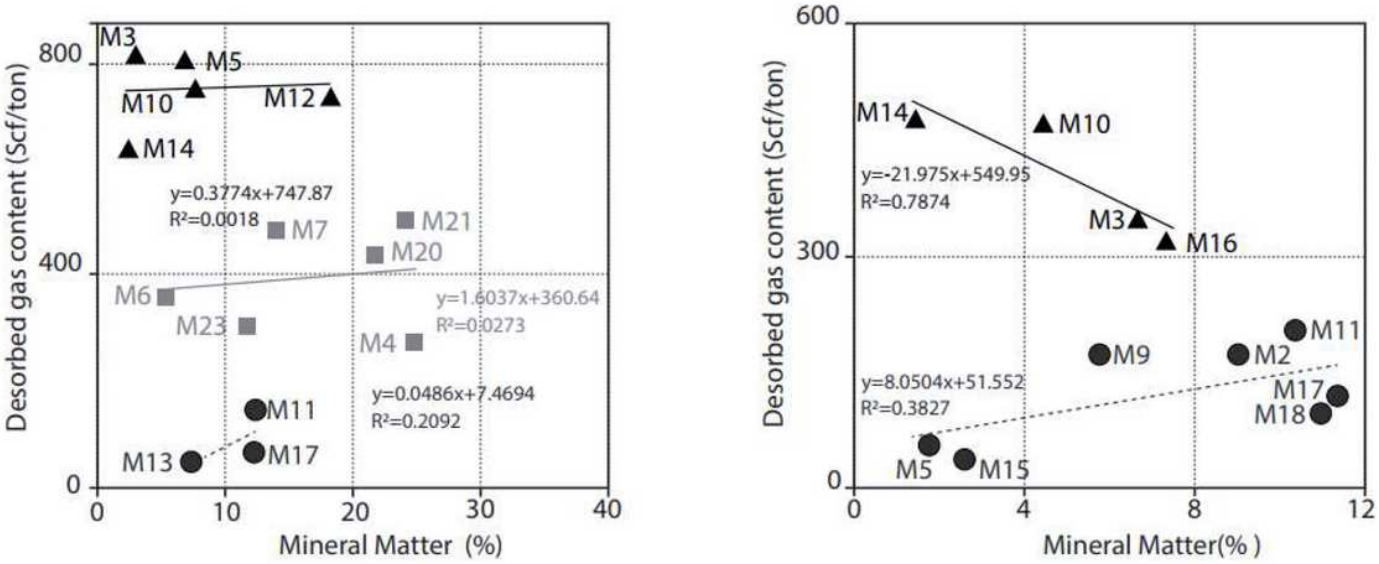

Figure 12

Relationship between mineral matter and the gas content (SCF/ton) (A). Landázuri 1 (B) Landázuri 2

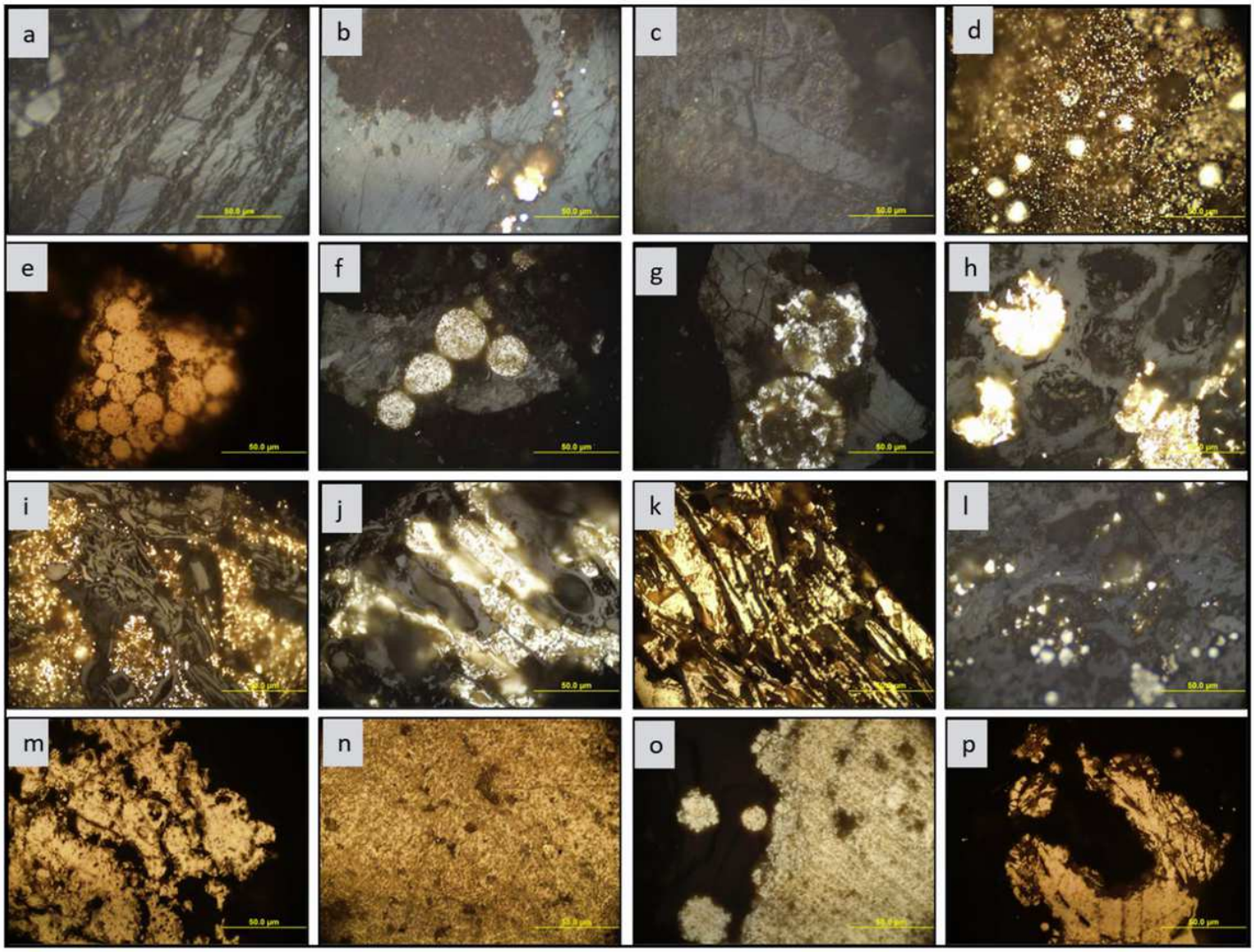

Figure 13

Microphotographs a. Clay minerals in M5- Landázuri-1, b. Clay minerals and pyrite -M17- Landázuri-2, c. Clay and others -M21- Landázuri-1, d. Framboidal pyrite -M17- Landázuri-2, e. Framboidal pyrite -M17-Landázuri-2, f. Framboidal pyrite -M7-Landázuri-1, g. Framboidal pyrite -M7-Landázuri-2, h. Syngenetic-diagenetic pyrite -M3-Landázuri-2, i. Epigenetic pyrite -M17- Landázuri-2, j. Epigenetic pyrite -M2-Landázuri-2, k. Epigenetic pyrite -M17-Landázuri-2, l. Syngenetic framboidal pyrite -M16-Landázuri-2, m. Diagenetic pyrite -M17-Landázuri-1, n. Diagenetic pyrite -M4- Landázuri-1, o. Diagenetic pyrite -M10-Landázuri-1, p. Late diagenetic pyrite? -M17-Landázuri-2.

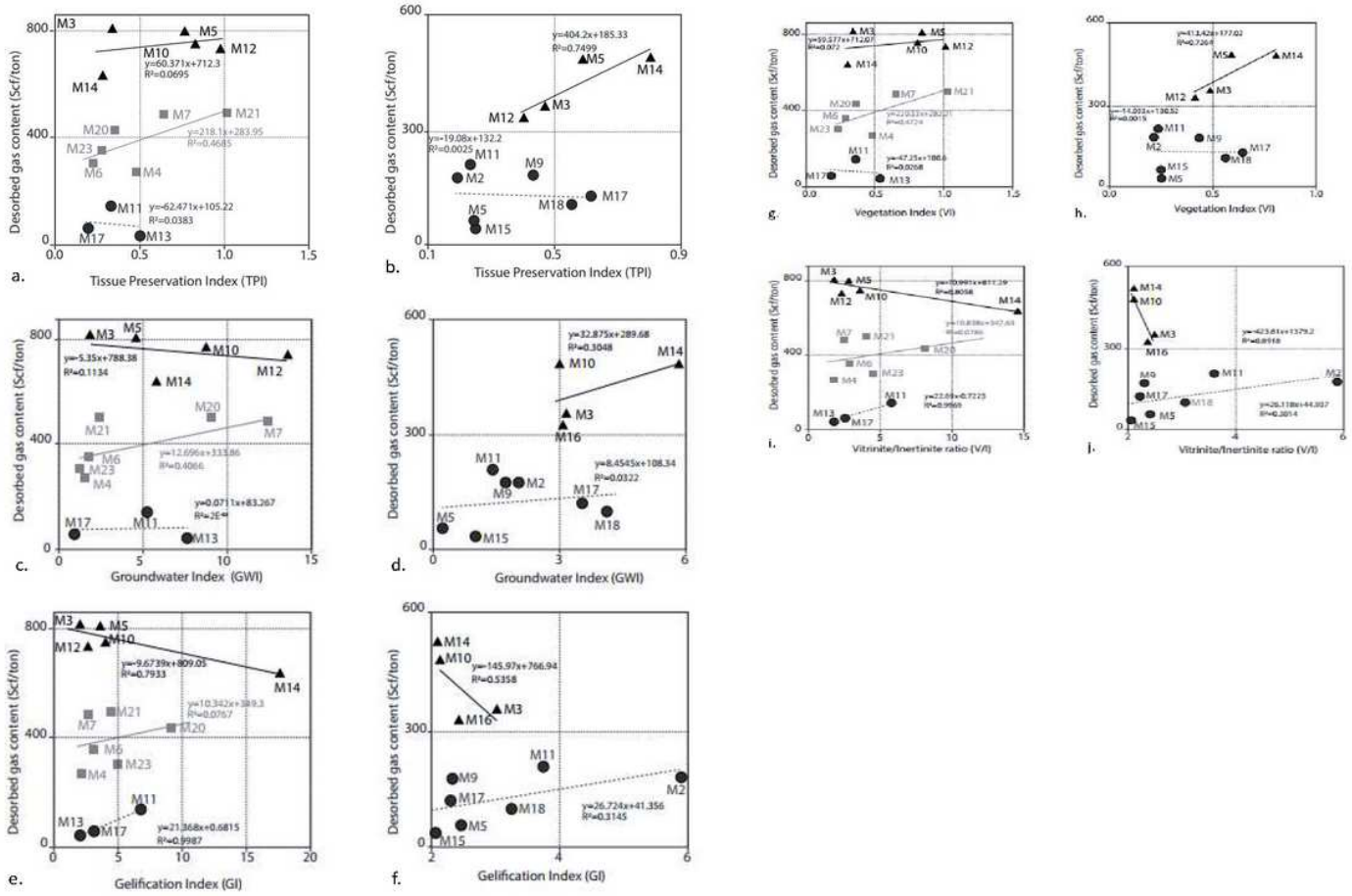

Figure 14

Relationships between gas content (SCF/ton) and petrographic indexes (TPI, GWI, GI, VI, and V/I).
Relationships between gas content (SCF/ton) and petrographic indexes (TPI, GWI, GI, VI, and V/I)

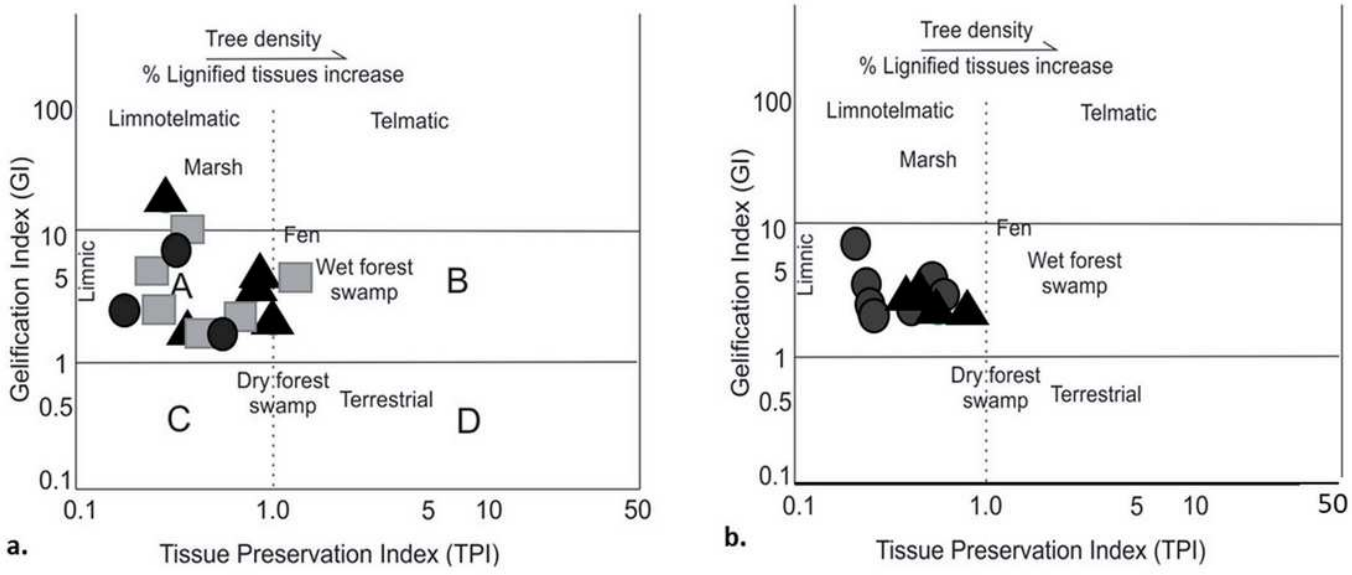

Figure 15

Coal facies (GI, TPI) Source: Diessel (1986) and modified by Kalkreuth et al. 1991. a. Landázuri 1. b. Landázuri 2 A. Vitrinite> Inertinite, Degraded Vitrinite> Structured Vitrinite B. Vitrinite> Structured Inertinite, Vitrinite> Degraded Vitrinite C. Inertinite> Vitrinite Inertodetrinite> Semifusinite- Fusinite D. Inertinite> Vitrinite Semifusinite+Fusinite> Inertodetrinite

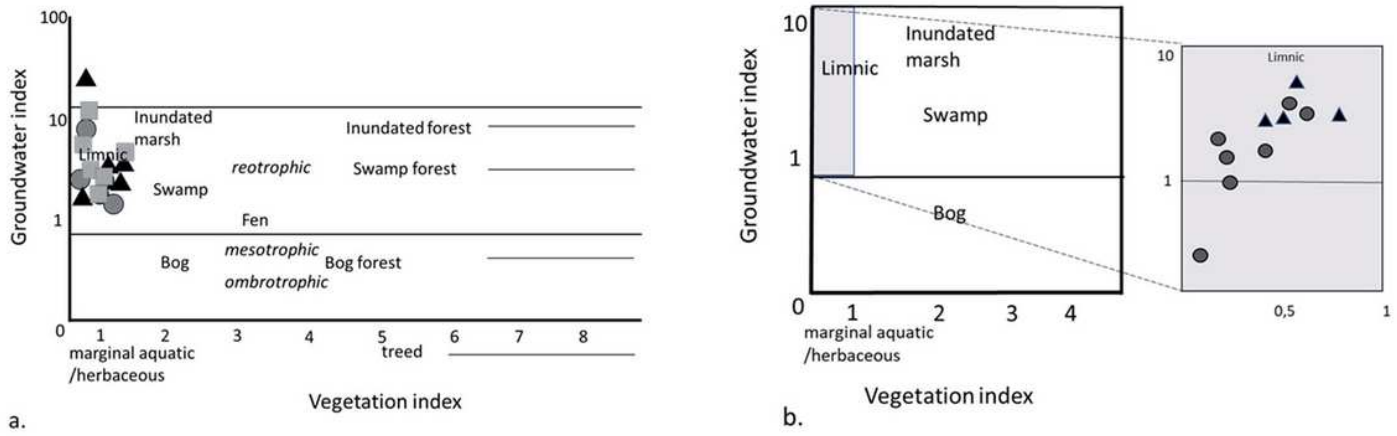

Figure 16

Coal facies (GWI, VI). a. Landázuri 1 b. Landázuri 2 (Modified from Calder et al., 1991)

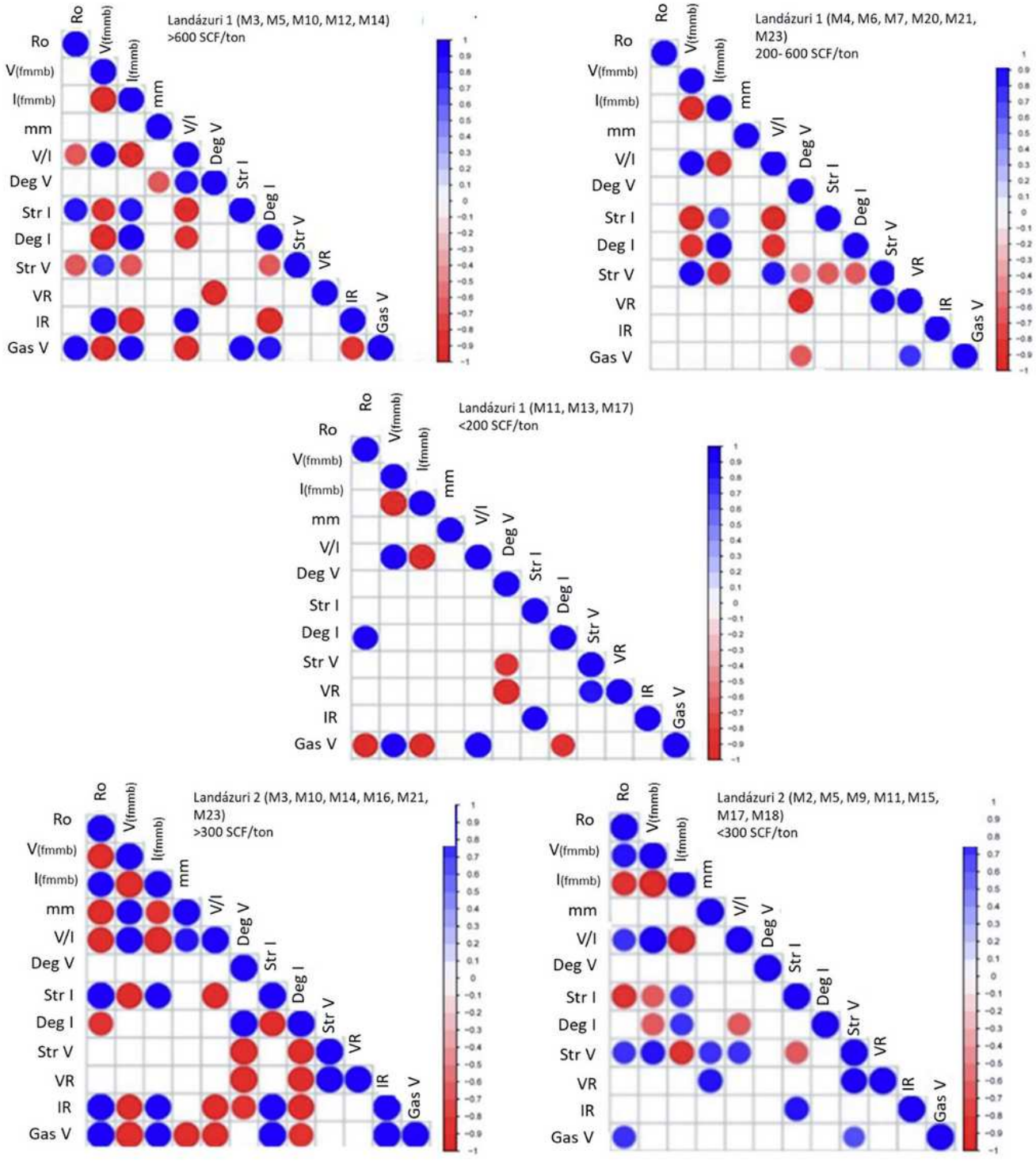

Figure 17

Pearson correlograms showing relationships between pairs of variables for Landázuri 1 and Landázuri-2 Ro- Average Vitrinite Reflectance, V fmmb - Vitrinite free mineral matter, I fmmb- Inertinite free mineral matter, mm- mineral matter, V/I- Vitrinite/Inertinite radius, Deg V- Degraded Vitrinite, Str I - Structured Inertinite, Deg I - Degraded Inertinite, Str V- Structured Vitrinite, RV- Vitrinite Radius, IR- Inertinite Radius, Gas V- Total gas volume measured SCF/ton

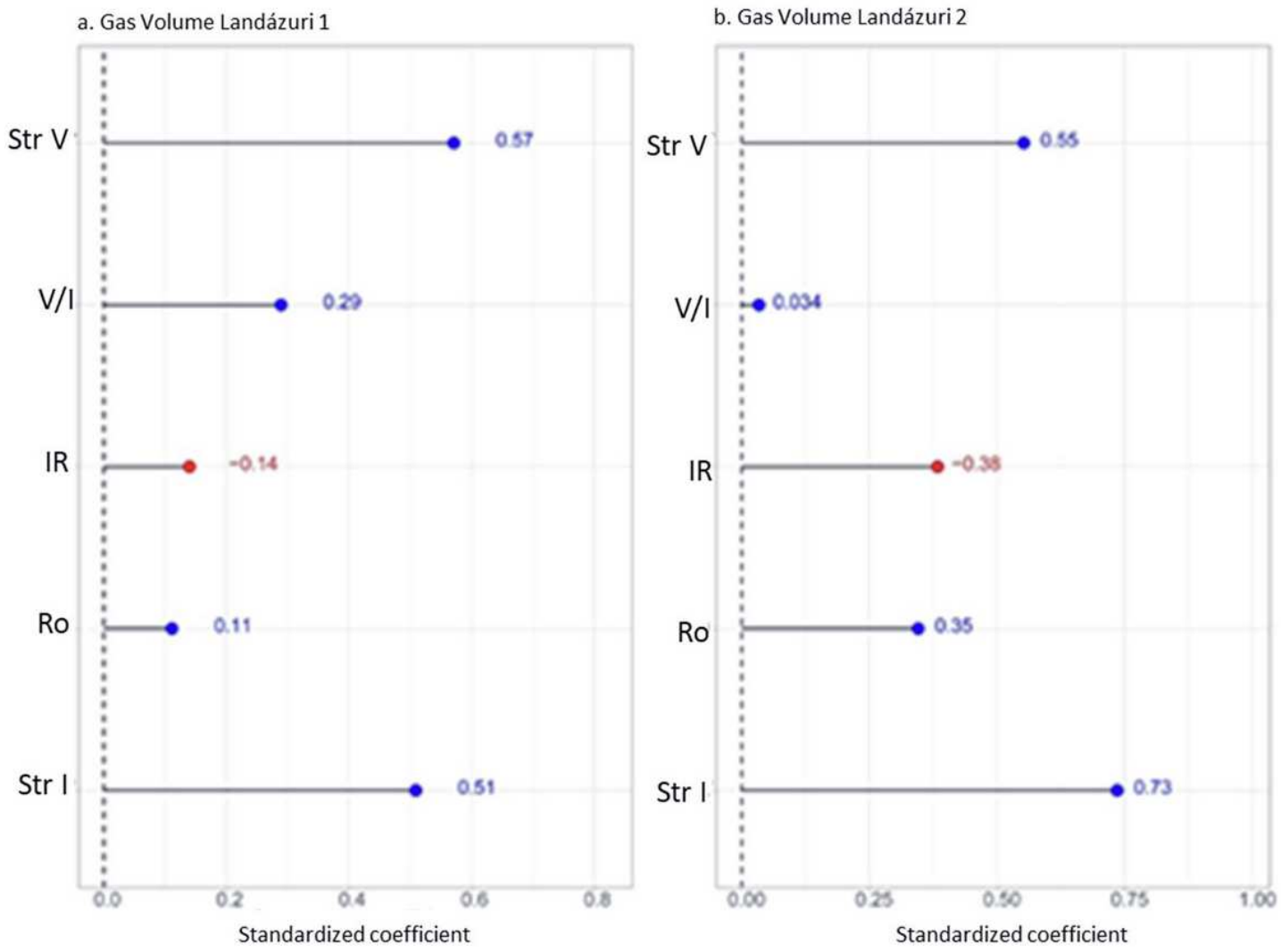

Figure 18

Behavior analysis of predictor variables (Str V, V/I, IR, Ro, Str I) versus response variable (Gas V) for the wells: a. Landazuri 1 and b. Landazuri 2

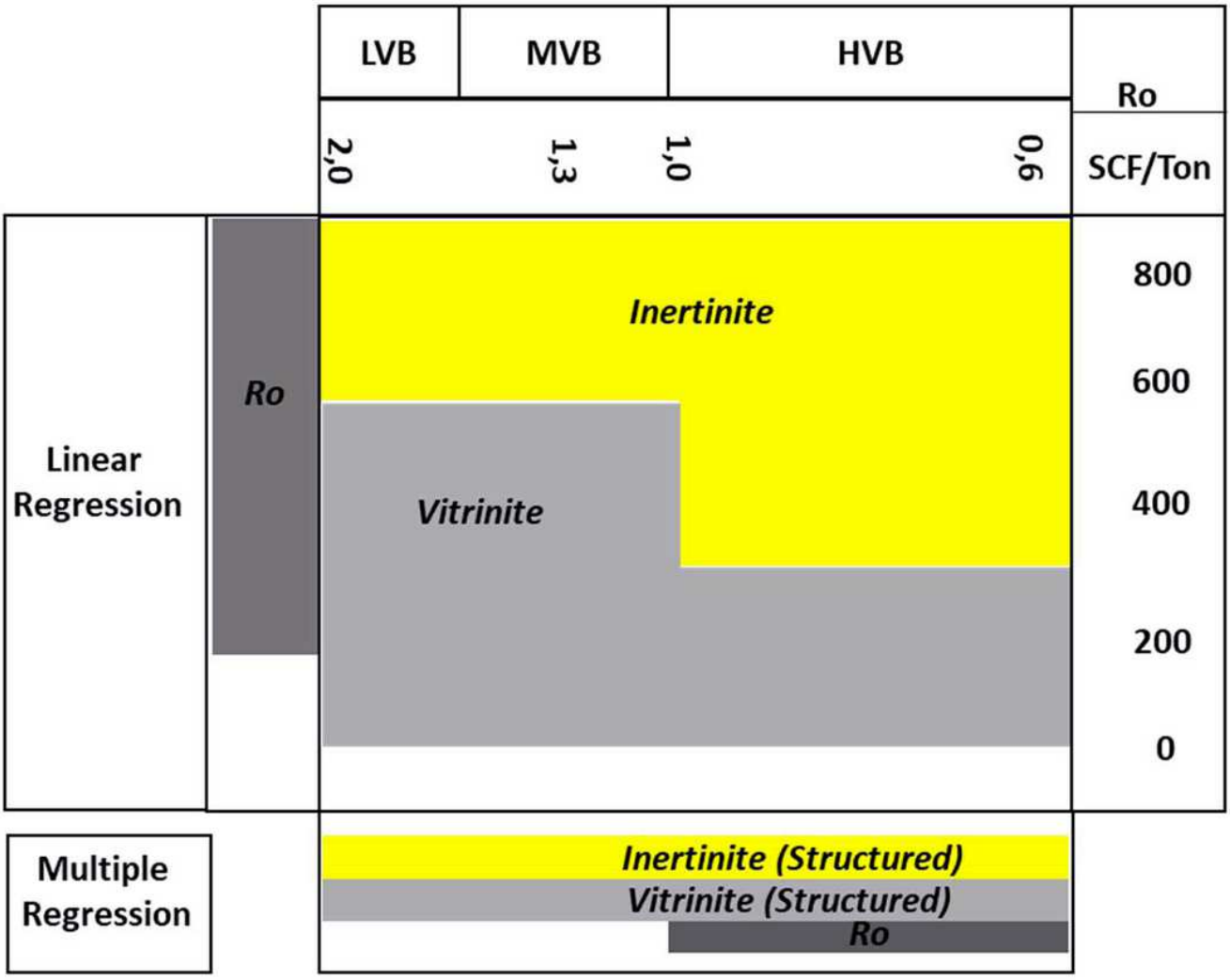

Figure 19

Synthesis of the importance of maceral groups and reflectance for the measured gas content

Supplementary Files

This is a list of supplementary files associated with this preprint. Click to download.

- GuatameetalTables.pdf